**Marine Geology**
March 2021, Volume 433 Pages 106405 (23p.)
https://doi.org/10.1016/j.margeo.2020.106405
https://archimer.ifremer.fr/doc/00665/77687/



# Coastal chalk cliff retreat rates during the Holocene, inferred from submarine platform morphology and cosmogenic exposure along the Normandy coast (NW France)

Duguet Timothée [1], Duperret Anne [1, *], Costa Stéphane [2], Regard Vincent [3], Maillet Grégoire [4]

[1] Normandie Université, UMR 6294 LOMC, CNRS, UNILEHAVRE, 53 rue de Prony, Le Havre 76600, France
[2] Normandie Université, UMR 6554 LETG-Caen, CNRS, UNICAEN, Esplanade de la Paix, Caen 14032, France
[3] Université de Toulouse, GET, CNRS, IRD, UPS, CNES, 14 Av. Edouard Belin, Toulouse 31400, France
[4] UMR 6112 LPG-Angers, CNRS, Université d'Angers, 2 boulevard Lavoisier, Angers 49000, France

* Corresponding author : Anne Duperret, email address : anne.duperret@univ-lehavre.fr

**Abstract :**

Submerged marine terraces potentially provide crucial information on past sea-level variations and paleo-coastline locations that may be used to estimate long-term coastal erosion rates. The Normandy coastline has recently been surveyed using a shallow water high-resolution mapping system. We identified a new continuous submarine platform, called the inner platform, limited by a shore parallel edge located between -9 m and -10 m (NGF) along the Normandy chalk coastline. A lower rock platform, called the outer platform, ranging from about -14 m to -17 m (NGF) appears locally. This corresponds to inherited preserved submarine terraces created during a past sea level highstand. The high cosmogenic 10Be concentration measured at the end of Mesnil-Val inner shore platform (including intertidal and subtidal shore platforms) is attributed to the last glacial cliff location at 6.5 ky ± 1 ky. From the spatial edge location of the inner platform in Normandy, we estimated cliff retreat rates since 6.5 ky ± 1 ky ranging from 0.051 ± 0.008 m/y to 0.090 ± 0.014 m/y from place to place. Comparisons with the current coastal chalk cliffs indicate a mean retreat rate estimated over the contemporary period suggesting such long-term retreat rates are 33% to 57% lower than the contemporary ones (0.10 m/y to 0.18 m/y). This confirms a contemporary acceleration of chalk cliff system retreat rates.

**Highlights**

► New detailed shallow bathymetry on Normandy chalk cliffs coast reveals the occurrence of steps on the submarine platform. ► The inter- and subtidal platforms analysis is realised using geologic successions, morpho-bathymetry and cosmogenic exposure. morpho- morphobathymetry. ► The high cosmogenic $^{10}$Be concentration measured on subtidal platform is attributed to the last glacial cliff location. ► The calculated Holocene cliffs retreat rates appear to be 33% to 57% less than the contemporary ones.

**Keywords** : Coastal cliffs, Chalk, Erosion, Rock platform, Holocene, Cosmogenic dating

## 1. Introduction

The erosion of the coastal chalk cliffs on the English Channel is a topic of great significance due to the natural hazards and risks induced by cliff collapses. Little is known about long-term (Holocene) cliff retreat rates, whereas the contemporary erosion rates have been estimated on both sides of the English Channel using different methods and over several periods. Analysis periods are constrained due to the scant availability of historical photographs and maps, reaching a maximal period of 150 years in the UK (Dornbusch et al., 2006, 2008) and 162 years in France, *i.e.* from 1824 to 1986 (Hénaff et al., 2002). Nowdays, the Normandy chalk cliff coastline is experiencing erosion rates of 0.10 m/y to 0.30 m/y (Costa et al., 2004; Letortu et al., 2014). Some recent methodologies based on cosmogenic dating ($^{10}$Be) were used in coastal marine environments and allow for the estimation of erosion rates over periods reaching several millennia. These methodologies were used on sites such as Normandy, France (Regard et al., 2012), in Korea (Choi et al., 2012), in East Sussex, UK (Hurst et al., 2016), in South Brittany, France (Raimbault et al., 2018a), and in Yorkshire, UK (Swirad, 2018). On the one hand, Regard et al. (2012) used $^{10}$Be dating at Mesnil-Val to quantify Normandy cliff erosion rates over 3000 years (0.11-0.13 m/y), which were found to be similar to the erosion rates of the contemporary period estimated with photogrammetry comparisons on the same study site over the last 42 years (0.15 m/y) (Costa et al., 2004; Letortu et al., 2014, 2015). Similarly, on the UK North Sea coast, Swirad (2018) using $^{10}$Be concentrations found a ~0.05 m/y millenial retreat rate in Whitby which is not significantly different from short-term rates (0.027+/-0.029 m/y calculated from 7 years of high resolution monitoring using terrestrial laser scanning (Rosser et al, 2013)). On the other hand, Hurst et al. (2016) extrapolated coastal cliff retreat rates for two sites on the East Sussex coast and covering most of the Holocene period. Retreat rates of 0.02-0.06 m/y were calculated from $^{10}$Be dating on a 250 m to 350 m wide platform on two sites. These long-term cliff retreat rates contrast with records obtained over the last 150 years of rapid retreat estimated from historical maps and photogrammetry comparisons (0.22-0.32 m/y) (Dornbusch et al., 2008). Hurst et al. (2016) concluded that contemporary retreat rates cannot be extrapolated back in time, and instead, cliff retreat rates must have recently accelerated to their observed values.

The aim of this paper is to precisely map coastal submarine platforms using high-resolution marine tools to determine and date, using $^{10}$Be, specific geomorphological features that are indicative of past cliff erosion processes. These long-term retreat rates will then be compared to contemporary ones to demonstrate whether the retreat of chalk cliff systems is increasing or not in Normandy.

Previous works on long-term cliff retreat using $^{10}$Be concentrations are based on a steady-state process of erosion that led to a continuous landward translation of the coastline with a similar shore platform shape and gradient, with the elevation of the cliff-platform junction (CPJ) tracking relative sea-level measurements (RSL) (Regard et al., 2012; Hurst et al., 2016, 2017). Hurst et al (2017) developed a simple numerical model for dynamic platform evolution (RoBoCoP model), which is broadly similar to those of Sunamura (1992), Anderson et al (1999) and Trenhaile (2000). The model assumes equilibrium retreat such that as the coast evolves the cross-section morphology remains steady while translating shoreward according to the prescribed retreat rate. The dynamic shore profile evolution model was coupled with predictions of $^{10}$Be production testing numerous exposure conditions such as block removal process, beach cover, topographic and water shielding, tide effect and relative sea level change (Hurst et al, 2017). The shape of the distribution of $^{10}$Be across the shore platform can potentially reveal whether cliff retreat rates are declining or accelerating through time (Hurst et al, 2017). Very recently, $^{10}$Be concentrations on shore platform in Yorkshire suggest steady state retreat, whilst maintaining a similar profile form, without direct relationship between relative sea level over centennial to millenial timescales and the erosion response of the coast (Swirad et al, 2020)

We have chosen to explore in detail four areas of the Normandy chalk coastline, including onshore and offshore topo-bathymetry, in order to assess the shore platform geomorphological variations. New high-resolution bathymetry surveys were reached near the coast using the shallow water R/V *Haliotis* with interferometric sonar mapping system (Geoswath).

Submarine coastal data shows the occurrence of a near-continuous and unrevealed submarine rocky platform with one or more submarine steps. One of these steps is parallel-oriented to the current coastline with a near-constant distance to the current cliff platform junction (CPJ) location. The geological analysis of the platform combined with cosmogenic nuclide ($^{10}$Be) concentrations were used to discuss the origin of the submarine steps and the modalities of long-term cliff retreat on the southern English Channel coast.

## 2. Materials and method

### 2.1. Normandy coastal and intertidal topography

The onshore part of the Normandy coastline was entirely and continuously mapped using aerial surveys provided by the French National Institute of Geography (IGN). Data are derived from the merging of several DEM data sets obtained using aerial LiDAR(RGEAlti®) and aerial photographs covering land, cliffs, and the upper portion of the shore platform, as a function of the tide level during surveys. The RGEAlti® DEM based on LiDAR data covers only a 2 km wide coastal fringe with a resolution of 1 m (horizontal) and a vertical accuracy of 0.2 m for land surfaces to 0.5 m for underwater surfaces.

### 2.2. Subtidal bathymetry

Swath shallow-water bathymetric data were obtained using the R/V *Haliotis* (IFREMER) during four cruises in order to map the submarine portion of the study sections. CROCOLIT-01 (Duperret, 2013a) covers the area offshore Ault, CROCOLIT-03 (Duperret, 2013b) covers a small area offshore Mesnil-Val, SPLASHALIOT-02 (Maillet, 2014) covers the area between Criel-sur-Mer and Mesnil-Val, and CROCO-CAUX (Duperret, 2017) covers the areas offshore the Cap d'Antifer cape up to Etretat and from Fécamp to Eletot (Fig. 1). In total, 309 bathymetric swath profiles with a total length of 680 km were created and cover an area of 31 $km^2$. All the raw data were obtained with the R/V *Haliotis* interferometric sonar (GeoSwath) that allows the acquisition of bathymetric data from shallow water depths ranging from 5 m to 30 m. Moreover, a chirp dataset was also obtained using a sub-bottom profiler (1.8 to 5.3 kHz) and 290 very high-resolution seismic profiles were treated with MATLAB and assessed with the KINGDOM suite software.  The vessel navigation was performed by RTK GPS (Real Time Kinematic Global Positioning System) using a reference station that provided a positioning accuracy of a few centimeters, located at a distance of less than 10 km away from the coast. Raw bathymetric data were later treated using CARAIBES software (©IFREMER) to (i) integrate the daily tidal variations during the acquisition, (ii) to clean the multibeam bathymetric profiles from outliers that can be attributed to boat turbulences and sea-surface agitation, and (iii) to create the offshore DEM by merging bathymetric profiles. The resulting offshore DEM has a horizontal resolution of 1 m and a vertical accuracy of 0.1 m.

The offshore bathymetric DEM and the onshore topographic DEM were finally merged in a single land/sea Digital Elevation Model and standardized to the national terrestrial reference origin (NGF), based on the Lambert93 French national projection system (ellipsoidal datum, GRS80).

Offshore lithological maps were then created, based on field work on coastal cliffs and shore platforms, dedicated to geological and lithological observations using key-marker stratigraphic correlations and on the geomorphological analysis of the bathymetry correlated with available borehole data from the coastal domain (BRGM database), indicating the depth of lithological formations and transitions.

### 2.3. Cosmogenic dating background

$^{10}$Be cosmogenic dating is based on the $^{10}$Be concentration produced by the interaction with the quartz-rich Earth surface. This *in-situ* concentration provides the exposure age to cosmic rays at the surface (Gosse & Phillips, 2001). In principle, any stable geological surface continuously exposed to cosmic rays will accumulate cosmogenic nuclides in surficial rocks over time (Lal, 1991; Dunai, 2010). $^{10}$Be production depends on the flux of cosmic rays, on the intensity of the terrestrial magnetic field, and on the absorption properties of the materials under study, controlled by the latitude and elevation of each sample.

The production of $^{10}$Be *in-situ* close to the surface declines exponentially with depth (self-shielding) as the cosmic ray flux taper off (Gosse & Phillips, 2001). We used $^{10}$Be dating to measure cosmic ray exposure by quantifying the accumulation of nuclides. The $^{10}$Be concentration determined in one sample depends on several factors (Regard et al., 2012), such as cosmic ray exposition duration, exposition depth, and ray shielding, such as vegetation, water or sediment cover.

## 3. Study sites and geological framework

Though the geology of the coastal chalk cliffs of Normandy has been fully explored by many authors (Mortimore & Pomerol, 1987, 1991, 1997; Costa, 1997; Mortimore, 2001, 2011; Costa et al., 2004, 2006; Duperret et al., 2002, 2004, 2005; Lageat et al., 2006; Senfaute et al., 2009; Letortu et al., 2015, 2019), the subtidal shore platform morphology remain largely unknown, except through large-scale bathymetry surveys (Augris et al., 1993; Augris et al., 2004) and local studies of intertidal shore platforms at Eletot and Les Grandes Dalles (Costa et al., 2006; Foote et al., 2006; Hénaff et al., 2006; Moses et al., 2006), and Mesnil-Val (Regard et al., 2012; Dewez et al., 2015; Duperret et al., 2016).

The Normandy coastal chalk cliffs are cut by two major northwest trending faults, the Fécamp-Lillebonne fault and the Bray fault. These major faults delineate three tectonic blocks (Fig. 1): from west to east, i) the Bec de Caux block with NNE dipping Cenomanian to Coniacian chalk, ii) the Caux block with the youngest chalk outcrops (Turonian to Campanian), and iii) the Picardy block made of Cenomanian to Turonian chalk folded along the Londinière and Bresle anticlines, and faulted by the Eu fault along the Bresle valley (Hauchard & Laignel, 2008; Duperret et al., 2012) (Fig. 1).

We chose to carry out an in-depth of four coastal sections with dissimilar Chalk Formations and consequently various physical properties. Each study site is located in a tectonic block along the Normandy coast, where various Chalk Formations outcrop: (1) in the Bec de Caux block section (Cap d'Antifer cape to Etretat), (2) in the Caux block section (from Fécamp to Senneville-sur-Fécamp), and (3) in the Picardy block section (from Penly to the town of Mesnil-Val, and a site offshore the town of Ault) (Fig. 1).

### 3.1. Cap d'Antifer cape and the Etretat coastal section

Along this section, the coastline trend varies on each side of  the Cap d'Antifer cape, with a north-south orientation to the south (from Saint-Jouin-Bruneval to the Cap d'Antifer cape) and a NE-SW orientation to the north (from the Cap d'Antifer cape to Etretat) (Fig. 1). The coastline is made of vertical chalk cliffs with heights varying from 90 m (Le Fourquet) to 70 m (Etretat).

From the Cap d'Antifer cape to Etretat, the NNE dipping of chalk units allows the exposure of a large diversity of Chalk Formations on the cliff section, including the Craie de Rouen Formation (Cenomanian), the Holywell Nodular Chalk Formation, the New Pit Chalk Formation (Turonian), and the Lewes Nodular Chalk Formation (Turonian-Coniacian) (Fig. 2). Cenomanian chalk units are exposed at the base of the cliff between the Le Fourquet and Antifer valley, and are characterized by coarse and nodular chalk with banks of harder beds (hardgrounds) (Duperret et al., 2012). The Upper Cenomanian Craie de Rouen is a white chalk with numerous flint bands and contains two main hardgrounds (hardgrounds Rouen 1 and 2) made of glauconitic and phosphate-cemented levels

(Juignet, 1974; Lasseur, 2007). Turonian chalk appears at the base of the cliff on the northwest side of the Antifer valley. It is composed of the Holywell Nodular Chalk Formation with very few flints and of local Antifer hardgrounds, as well as by the massively bedded chalk of the New Pit Formation that contains several marl seams and hardground layers, called the Three Tilleul hardgrounds (Mortimore & Pomerol, 1991). The Lewes Nodular Chalk Formation outcrops at the base of the Etretat cliff as a coarse chalk with many nodular chalk beds and flints, dated from the Upper Turonian to Lower Coniacian (Mortimore et al., 2001). Locally, the Lewes Nodular Chalk is called the Etretat complex, and is related to a major Cretaceous tectonic phase (Mortimore & Pomerol, 1987) and shows numerous hardgrounds and flint levels (Fig. 2).

### 3.2. Fécamp to Eletot coastal section

The coastline trend varies on each side of the Cap Fagnet cape (Fécamp), with a N30° orientation on its west side (from south Fécamp to the Cap Fagnet cape) and a N60° orientation on its east side (from Cap Fagnet cape to Eletot) (Fig. 1).

Chalk cliffs in the Fécamp area have been largely surveyed due to the occurrence of the Fecamp-Lillebonne normal fault (Mortimore & Pomerol, 1987; Lasseur et al., 2009; Duperret et al., 2012), which exposes the complete Upper Cretaceous stratigraphic succession from the Craie de Rouen (Cenomanian) to the Seaford Chalk Formation (Coniacian) (Fig. 2), up to the top of the 105 m high Cap Fagnet cape cliff. At Senneville-sur-Fécamp, the cliff base is made of the New Pit Chalk Formation with specific Tilleul hardgrounds. At Eletot, the cliff base exposes a specific unit of the Lewes Nodular Chalk Formation dated from Late Turonian and called the “Chalk Rock” unit (Mortimore, 2001). On this coastal section, the Seaford Chalk Formation appears at the top of the cliff as a homogeneous soft chalk with regular flint levels dating from the Middle Coniacian to the Middle Santonian (Fig. 1).

### 3.3. Penly / Biville-sur-Mer to Mesnil-Val coastal section

The coastline trend is N60°E from Biville-sur-Mer to the westside of the Yères valley and becomes N50°E east of the Yères valley, from Criel-sur-Mer to Mesnil-Val (Fig. 1). Both the cliff and shore platforms of the Mesnil-Val site have already been surveyed (Senfaute et al., 2009, Regard et al., 2012; Dewez et al., 2013, 2015; Duperret et al., 2016) by the European and French research projects dedicated to this site.

The cliff section from Biville-sur-Mer to Mesnil-Val is made of the Holywell Nodular Chalk Formation (Turonian) with the occurrence of New Pit Marls at the base of the cliff located on the south side of Criel-sur-Mer, and the Lewes Nodular Chalk Formation (Late Turonian) that outcrops at the base of the Mesnil-Val's cliff (Fig. 2). Criel-sur-Mer is crossed by the N-S Yères valley carved along the N-S axis of the Criel-sur-Mer syncline along the south side of the Bresle anticline axis at Le Tréport (Fig. 1). The same chalk unit formations thus appear on each side of the Yères valley at Criel-sur-Mer.

### 3.4. Ault coastal section

The cliff section in the Ault area is only composed of the Lewes Nodular Chalk Formation (Lower Coniacian) and the overlying Seaford Chalk Formation (Coniacian), with a continuous NE dip (Fig. 1). The Ault cliff height decreases progressively from 60 m in the southwest to sea-level in the northeast, and so on until the end of the chalk cliffs coastline.

## 4. Hydrodynamic and climatic conditions

Marine and climate processes are key factors of coastal cliff evolution. For example, waves may break directly on the cliff base during high spring tides and allow the debris stuck at its foot to be removed. This leads to the continuous instability of the cliff face (Trenhaile, 1987, 2000; Sunamura, 1977, 1992; Peregrine & Kalliadasis, 1996; Brossard & Duperret, 2004; Costa et al., 2006; Lim et al., 2011; Young et al., 2011). Furthermore, continental processes such as rainfall also contribute to cliff collapses from chemical and physical alteration such as chalk dissolution (Rodet, 1983; Duperret et al., 2002) and an increase of water pore pressure (Duperret et al., 2002; Costa et al., 2004).

During astronomical spring tides, the Normandy chalk coastline has a tidal range of 8.12 m at Le Fourquet and 10.21 m at Le Tréport (SHOM, 2017). Long period waves and waves with significant amplitudes were recently recorded offshore Penly at the real-time directional Penly buoy (anchorage at 11 m depth) from November 2017 to January 2019 (CEREMA, 2019). The rose diagram illustrates a main NW swell (from N280°E to N300°E) with a mean significant wave height of 1 m and a period of

4.8s (Fig. 1). Only 10% of the recorded swell data shows a period that is longer than 7s and a height that is higher than 1.5 m. Nevertheless, the Penly buoy has recorded extreme significant wave heights of 4.5 m, with a period of 10.8 s, for example during the Eleanor storm ($3^{nd}$ and $4^{rd}$ January 2018). During the storms (in December 2017, 2019, January 2018, February 2020), a maximum wave height of 7-8m have been recorded. Additionally, some 0.5-1 m high northern waves may also occur during winter.

The Normandy region is subject to an oceanic climate with a mean annual minimal temperature of 8.9°C and a mean annual maximal temperature of 13.9°C (established between 1981-2010 at Cap de la Hève station, Le Havre, Météo-France). Rainfall are rather well spread out throughout the year (≈ 800 mm) with a generally wetter winter period (averages of 52 mm in July and 88 mm in December).

## 5. Inter- and subtidal shore platforms

The shore platform is defined as a gentle rock slope extending between the high astronomical tide (HAT) and the low astronomical tide (LAT) (during spring tides). As defined in the coastal domain of SW Brittany, the offshore submarine extension of the shore platform is called the rock platform, due to its pluri-kilometric cross-shore extension (Raimbault et al., 2018b). Shore (intertidal) and rock (subtidal) platforms appear on all Normandy coastal land-sea DEMs, butonly four study sections have been assessed and compared using detailed bathymetry maps and chalk lithology datasets in order to explore the complete inter- and subtidal platform system. Study sections cover 9.5 $km^2$ between the Cap d'Antifer cape and Etretat, 6.5 $km^2$ between Fécamp and Eletot, 10.1 $km^2$ between Biville sur Mer and Mesnil-Val, and 1.8 $km^2$ in Ault (Fig. 1). The new detailed bathymetric maps reveal continuous geomorphological steps. These are studied in order to find their origin.

### 5.1. Cap d'Antifer cape to the Etretat section

#### 5.1.1. Shore and submarine morphology

The land-sea DEM cover 9.5 $km^2$ and the bathymetric dataset extends from 1 km offshore Le Fourquet to 2 km offshore Etretat, and up to 20 m in depth (NGF) (Fig. 3a). Bathymetry reveals a 100 to 200 m wide shore platform with a lower limit (LAT level) roughly parallel to the coastline, though some bathymetric data are lacking in this area due to the imperfect coverage of the aerial and bathymetric surveys (Fig. 3a). The land-sea DEM focused on the Fourquet headland shows the shore platform extending from the shingle beach bar (5 m NGF) to LAT level (Fig. 3b). Shingle cover is confined to the uppermost part of the shore platform near the CPJ, roughly extending from 0 to 5 m (NGF). Some large chalk debris from cliff collapses remain on the beach near the cliff. At about -2 m (NGF) we observe a change in the surface texture of the shore platform, from a smooth surface to runnels.. The intertidal smooth surface results from the vertical accuracy difference between the aerial LiDAR dataset, the RGEAlti DEM on shore ( 0.5 m), and the submarine GeoSwath dataset (0.1 m).

One step ($S_0$) delineates the Fourquet headland base and appears again at the Manneporte arch base to extend offshore Etretat (Fig. 3b & Fig. 3c). $S_0$ begins on the shore platform and extends underwater in the subtidal area. The $S_1$ step is a limit between the runnelled subtidal platform and underlying non-runnelled subtidal platform (Fig. 3c), while the $S_2$ step represents the boundary of the lowest flat and smooth surface (Fig. 3c).

The rocky surface extends in the submarine domain and consists of a rock platform with progressive width variation, ranging from 310 m at Le Fourquet to 1200 m offshore Le Tilleul (Fig. 3). We marked the inland geomorphological limit of the platform at the Cliff-Platform Junction (CPJ, Wright, 1970), located onshore at 0.5 m (NGF), and the offshore limit at the top of the step (called $S_2$) located at a depth of -17 m (NGF) (Fig. 3). The 2 m high $S_2$ step marks the subtidal platform edge that represents the submarine limit between the rock platform and a 0.5 to 1 m thick sediment cover made of quaternary gravels and sand, also previously observed (Larsonneur et al., 1979; Augris et al., 2004) (Fig. 3c). South of Cap d'Antifer cape, the $S_2$ step is roughly parallel to the intertidal shore platform and the present-day coastline, but the $S_2$ trend gradually evolves northward to reach a north-south trend offshore le Tilleul, whereas the coastline and the intertidal platform are SW-NE oriented (Fig. 3a). $S_2$ is not observed between Le Tilleul and Etretat, where recent sediments, locally 1 to 3 m thick, cover the distal part of the subtidal platform (Augris et al., 2004) (Fig. 3c). The rock platform is split into two geomorphological units limited by a step ($S_1$) that could be considered as an edge (Fig. 3). We propose to name the lower part of the subtidal platform located below $S_1$ the outer platform, and its upper part, located above $S_1$, the inner platform (including subtidal and intertidal shore platforms) (Fig. 3c). The outer platform is a surface with low rugosity and slope gradient lower than 1°, extending from

$S_2$ to the base of $S_1$ around -17 m to -13 m (NGF) (Fig. 3c & Fig. 4b). Its width reaches 900 m offshore Le Tilleul and is gradually covered by sediments eastward (Fig. 3c).

The inner platform extends from $S_1$ (-10 m NGF) up to the CPJ (0 to 1 m NGF), with a width varying from 280 m (La Courtine) to 400 m (Porte d'Aval) (Fig. 3a). The inner platform is steeper than the outer platform (1.5° to 1.9°) and entirely bare (Fig. 3c). Furthermore, the $S_1$ runs nearly parallel to the coastline, except offshore the Etretat valley outlet (Fig. 3a).

Finally, the shore platform $S_0$ steps can only be found near Le Fourquet and Etretat. They correspond to intertidal steps locally developed around the Fourquet headland and linked to the low-tide sea-level with a hardground level in the Craie de Rouen Chalk Formation (Fig. 4). In Etretat, $S_0$ is a 3 m high step located on the rock platform under the LAT level (Fig. 3c). At this location, the $S_0$ step corresponds to the contact between the Lewes Nodular Chalk and New Pit Chalk Formations, as revealed by the stratigraphic succession observed at the cliff face headland.

**5.1.2. Submarine and shore geology**

A borehole BRGM-1 (BRGM database) drilled in the Antifer valley at Le Tilleul (BRGM, 1970) illustrates the following lithological succession: (i) the Craie de Rouen Formation from 0 to -12 m (NGF), (ii) the sandy Glauconitic Chalk Formation relating to the Cenomanian down to about -16 m (NGF), and (iii) the Albian clayey limestones below, also called Gaize (Juignet, 1974). A second borehole BRGM-2 (BRGM database) located in the Etretat valley revealed evidence of Lower Coniacian chalk from -1.2 m to -9.1 m (NGF) and Upper Turonian chalk down to -16.2 m (NGF) (BRGM, 1963). Along the section from Le Tilleul to Etretat, the overall regional NE dip of chalk strata (Mortimore, 2001, 2011; Duperret et al., 2012) is interrupted by a gentle syncline between Fourquet Point and the La Courtine arch, followed by an anticline up to the Valaine location (Fig. 4a). Nevertheless, the regional structure allows us to draw a geological map for the inner platform, as a function of geomorphological variations, apparent dips of structures, and BRGM boreholes (Fig. 4a). From southwest to northeast, the inner platform is shaped in the Craie de Rouen Formation offshore the Cap d'Antifer cape, Le Fourquet, Le Tilleul including the Courtine point, and then changes to the Holywell Nodular Chalk Formation from the La Courtine arch to the Manneporte arch, the New Pit Chalk Formation between the Manneporte arch and the Porte d'Aval arch, and then finally the Lewes Nodular Chalk Formation offshore the Etretat valley (Fig. 4a). The locations of the local arches such as the Porte d'Aval, the Manneporte, and the Courtine arches are associated with hard chalk formations, corresponding to the New Pit, the Holywell Nodular, and the Craie de Rouen Chalk Formations, respectively (Fig. 4a). The large-scale Antifer cape, where the current coastline is changing trends, is cut within the Craie de Rouen Formation. On this section, the edge of the inner platform ($S_1$) is roughly and continuously oriented parallel to the current coastline. The outer platform limited by the $S_2$ edge extends mainly between Cap d'Antifer cape and Le Tilleul valley. The outer platform is partially made of the Craie de Rouen Formation in its upper part and of the Glauconitic Chalk Formation from -12 m to -16 m (NGF), which is easily recognisable given the apparent SW dipping of indurated chalk strata with glauconite (Fig. 4a & Fig. 4b). The inner platform edge, $S_1$, crosses three various chalk formations, starting from the Glauconitic Chalk Formation, the Craie de Rouen Formation, and the Holywell Chalk Formation (Fig. 4a). Therefore, $S_1$ step is not related to a lithological change, but to an erosive process of the rock platform. However, $S_2$, located -17 m offshore Le Tilleul, appears to follow geological strata (Fig. 3c) and corresponds to the contact between the Glauconitic Chalk Formation and the underlying Albian clayey limestones (Gaize Formation) as observed from lithological successions reported from the borehole BRGM-1.

### 5.2. Fécamp to Eletot section

#### 5.2.1. Shore and submarine morphology

Along the coastal section from Fécamp to Eletot bathymetry data extends up to 1 km offshore to a depth of 18 m (NGF) (Fig. 5a). The shore platform is a relatively flat (1° slope gradient) and narrow (200 to 250 m wide) surface with a low rugosity, limited offshore by the LAT level position, sub-parallel to the coastline (Fig. 5). A few meters below the LAT level, 2 m high steps ($S_0$) appear locally, among some other steps, especially around the Cap Fagnet cape (Fig. 5b). Herein, $S_0$ is a hardground level (more indurated than the surrounding chalk) in the Craie de Rouen Formation as observed in the field on the shore platform at the Cap Fagnet cape (Fig. 5b) and in Senneville-sur-Fécamp (Fig. 5c).

Along this coastal section, the intertidal shore platform is a smooth surface with some blocks, whereas the subtidal rock platform shows a lot of runnels with a similar NW-SE trend, only developing along the inner platform (CPJ to $S_1$) (Fig. 5c). $S_1$ may be represented locally by a vertical step similar to offshore Eletot where the step is progressively covered eastward with sediments, otherwise $S_1$ may present a slope similar to offshore Senneville-sur-Fécamp (Fig. 5c). Like in the previous coastal section, $S_1$ is located at around -10 (NGF) but herein without outer platform development. $S_1$ represents the edge of the inner platform and marks the contact with the offshore sediment cover (Fig. 5c). $S_1$ is ongoing and almost near parallel-oriented to the coastline except offshore the Valmont valley outlet where the paleo-river drainage incised the valley to below $S_1$.(Fig. 5a). The subtidal rock surface gradually widens from 370 m at in the Cap Fagnet cape to 590 m in Eletot with a 1.8° to 1.2° slope gradient (Fig. 5a & Fig. 6b).

Offshore Senneville-sur-Fécamp, the $S_1$ trend is roughly parallel to the coastline, except where $S_1$ is interrupted by a scar with paleo-scree deposits, made of big boulders partially covered with sediments (Fig. 5a). The estimated length of the chalk debris deposited appears to reach 150 m out to sea with a surface of 29 000 $m^2$ (Fig. 5a). Such lengths of chalk debris deposits are equivalent to those observed from modern collapses on the chalk cliffs of Normandy (Duperret et al., 2002, 2004). In this case, this offshore debris can be the result of a cliff collapse that occurred when the cliff and the paleo-coastline was right at the $S_1$ location.

Along this coastal section of Normandy, the inner rock platform morphology appears as a succession of 3-4 superposed and short (50 m mean width) rock surfaces, all limited by small edges of various trends. Such a configuration may be linked to the occurrence of numerous superposed hardground levels in the Craie de Rouen Formation, favouring guidance for step back-wearing (Fig. 6b) (Dornbusch & Robinson, 2011; Regard et al., 2013; Dewez et al., 2015).

**5.2.2. Shore and submarine geology**

The borehole BRGM-3 (BRGM database) drilled in the Fécamp harbour shows an Upper Cenomanian Glauconitic Chalk Formation, from -10 m (NGF) to the core bottom (-17 m NGF) (BRGM, 1969), and field observations of the shore platform below the Cap Fagnet cape show the overlying Craie de Rouen Formation. On the western side of the Valmont valley, field observations show the Lewes Nodular Chalk Formation from Coniacian to Turonian (Fig. 6a). The stratigraphic offset of the chalk outcrops of the cliffs and the shore platforms on each part of the Valmont valley (Fécamp) is a strong argument to the location of the Fécamp-Lillebonne fault in this area (Mortimore & Pomerol, 1987; Lasseur et al., 2009; Mortimore, 2011). There is no offshore morphological track of such a fault on the rock platform, especially on the western limit of the Fécamp rock platform, due to the Valmont valley outlet that is infilled with sediment and cuts the rocky platform offshore Fécamp (Fig. 6a).

Nevertheless, the stratigraphic offset observed between the Lewes Nodular Chalk Formation (Turonian-Coniacian) and the Glauconitic Chalk Formation (Cenomanian) is relative to the Fécamp-Lillebonne fault occurrence with a local N170E trend in the offshore prolongation of the south side of the Valmont valley (Fig. 6a). At the Cap Fagnet cape, the NE strata dip brings the coarse Craie de Rouen Formation to the rock platform surface and cliff toe level (Fig. 6a & Fig. 6b). The overlying Holywell Nodular Formation appears at the beach level east of the northern point of the Cap Fagnet cape and shapes the rock platform up to Senneville-sur-Fécamp (Fig. 6a). In Senneville-sur-Fécamp, the contact between the Holywell Nodular and New Pit Chalk Formations is underlined by step $S_0$, crossing the shore and the rock platforms until $S_1$ and is easily recognizable in the field and on the bathymetry (Fig. 6a).

### 5.3. Biville-sur-Mer to Mesnil-Val section

#### 5.3.1. Shore and submarine morphology

The bathymetric dataset (CROCOLIT-2013 and SPLASHALIOT-2014 cruises) extends to 1.5 km offshore down to -20 m (NGF) from Biville-sur-Mer to Mesnil-Val (Fig. 7a).

In Criel-sur-Mer, the shore platform is narrow (300 m wide to the LAT limit) and smooth with a slope gradient of 1.4° (Fig. 7b), whereas northeast of Mesnil-Val, the shore platform is wide (435 m), flatter (0.8°) and rougher, with many steps and runnels. The shore platform of Mesnil-Val is locally known as the Muron Rocks (Duperret et al., 2016) where $^{10}$Be cosmogenic dating has been explored by Regard et al. (2012) in order to estimate the long-term cliff retreat rate.

Like the previous sections, the rock platform from Biville-sur-Mer to Mesnil-Val extends below the LAT level and shapes the inner platform, limited by edge $S_1$ (Fig. 7b & Fig.7c), is ongoing and oriented parallel to the shore and the coastline, except on the Muron Rocks where the inner platform is larger (800 m) (Fig. 7a). The inner platform is herein a bare gentle slope surface from 0.7° in Mesnil-Val to 1.2° from Criel-sur-Mer to Biville-sur-Mer with a corresponding width of 800 m to 500 m. The inner platform edge ($S_1$) is a sloping edge located between -9 and -10 m (NGF) (Fig. 8b). No outer platform is perceptible beyond $S_1$ (Fig. 7c). $S_1$ represents the boundary between the bare rock platform and the underlying sediment cover (Fig. 7b & Fig. 7c). Finally, some other higher steps ($S_0$) are located on the rock platform but are not continuous and parallel to the coastline. Like the other coastal sections, they mainly correspond to hardground levels of the chalk where the erosion process has been amplified, as already suggested here (Dewez et al., 2015; Duperret et al., 2016) (Fig. 8b).

#### 5.3.2. Submarine and shore geology

The borehole BRGM-4 (BRGM database) drilled in the Yères valley axis shows at -0.6 m (NGF) (BRGM, 1956) the Coniacian to Turonian limit represented by the Lewes Marl key-marker within the Lewes Nodular Chalk Formation (Fig. 2). In Criel-sur-Mer, the coastline is cut by a N-S syncline favouring the Lewes Nodular Chalk Formation, outcropping with older chalk units underneath (New Pit Chalk Formation) on each side of the syncline, both offshore Mesnil-Val and Biville-sur-Mer (Fig. 8a & Fig. 8b). The Yères valley is developed along the axis of the syncline and the Muron Rocks may be considered to be the eastern border of the syncline, surfacing during LAT periods (Fig. 8a). As also observed offshore Etretat, the $S_1$ step is not present offshore the outlet of the Valmont valley.

Furthermore, at 3.8 km westward from the studied coastal section (offshore Penly) (Fig. 9), the chalk rock basement was estimated to be around -15 m (NGF), below a 1 m to 5 m thick Pleistocene sedimentary cover on two offshore boreholes, BRGM-5 and BRGM-6 (BRGM database) (BRGM, 1993) (Fig. 9). The chalk basement has been also reported on the Chirp profile Splash33 under the Pleistocene sand cover (Fig. 9). The BRGM-6 borehole is located immediately below the $S_1$ edge that bounds the inner and outer rock platform (Fig.9).

### 5.4. Ault section

#### 5.4.1. Submarine morphology

The bathymetry dataset extends until 800 m offshore Ault down to a depth of 12 m (NGF) (Fig. 10a). A 300 m wide, smooth and flat shore platform (1°) is observed along the coastal section (Fig. 10b). The Ault area is the only coastal section where the shore platform is partially covered with sediments that are widely present in this area neighbouring the Somme estuary. Sand isopachs have been generated from Chirp profile interpretations (CROCOLIT_01 cruise). A 1 to 14 m sediment cover is visible and increases to the northeast (Fig. 10d). A map of the chalk basement elevation has been made and the top of the chalk deepens northeastward down to -20 m (NGF) (Fig. 10c). Figure 10c represents the portion of the submarine rock surface without sediment coverage; it is a gently sloped surface (0.7°) ending with a sloping edge ($S_1$) where its top is located at about -9 m (NGF) (Fig. 10c). As defined in the previous coastal sections, this surface corresponds to the inner platform ended by edge $S_1$. The inner platform width ranges from 450 m in the north of Ault to more than 800 m southward, where $S_1$ is beyond the bathymetric data cover (Fig. 10c). The inner platform width decreases progressively to the northeast, corresponding to the similar aerial disappearance of cliffs at Ault, ending the Normandy chalk cliffs coastline.

#### 5.4.2. Submarine and shore geology

The BRGM-7 borehole (BRGM database) made in the north of Ault reveals the Upper Turonian Formation of the Lewes Nodular Chalk Formation to the core bottom at -6 m (NGF) (BRGM, 1973). As the edge of the inner platform ($S_1$) is located at -9 m (NGF), only 3 m deeper than the BRGM-7 borehole bottom, the entire inner platform is made of Lewes Nodular Chalk Formation (Fig. 10d).

## 6. Normandy marine platform model

### 6.1. A common structure

The marine platform observed along the four distinct coastal sections display common characteristics (Fig. 11). A gently dipping surface (1-2° dip) that starts at the CPJ located at 0 to 2.5 m (NGF) down to a distal edge, the morphological edge ($S_1$), and sometimes extended to the lithological step $S_2$ as observed at -17 m (NGF) along the Antifer to Etretat section. $S_1$ is observed on all coastal sections and it can be either a vertical step or a slope gradient, and is linear and nearly parallel to the present-day coastline. $S_1$ is continuous along the coastline, except offshore the outlets of large-scale valleys crossing the coastline, such as offshore the Etretat valley, the Valmont valley at Fécamp, and the Yères valley at Criel-sur-Mer. There, $S_1$ may have been eroded by river incision. The top of $S_1$ is always located between -9 m and -10 m (NGF), despite the lithology and the structuration of the chalk. It may split the rock platform in two parts, as observed locally at Antifer, with an upper platform from the CPJ to the top of $S_1$, named the inner platform, and a lower platform from $S_1$ to the top of $S_2$, named the outer platform. The inner platform has a slope gradient varying from 0.8° to 2.1°, and extends into the intertidal area (the shore platform) and the subtidal area. The outer platform is partially covered by sediments, as evidenced by the seismic profile acquired near Penly (Fig. 9). The outer platform of Antifer extends exclusively in the subtidal domain from the base of $S_1$ (~ -15 m) to the top of $S_2$, with a slope gradient varying from 0.3° to 1.2° (Fig. 11). The appearance of a rocky and bare outer platform only located offshore the Cap d'Antifer cape may be explained by high marine hydrodynamics in this area that inhibit sediment accumulation down to a minimal depth of -17m (NGF). This is confirmed by a drastic change in coastal drift from this point of the coast, from southwest to northeast. As observed in the field, such as on the shore platform of Mesnil-Val, the inner rock platform shows numerous steps, called $S_0$ (Fig.11). Field work shows they correspond to small-scale sedimentological facies variations of the chalk, such as hardground levels or the Chalk Formation lithological limits described on the Mesnil-Val shore platform (Regard et al., 2012; Dewez et al., 2015; Duperret et al., 2016). In Normandy, the inner platform is always made of bare chalky rocks except in the Ault area, in the northernmost section, where sediments coming from the Somme estuary are progressively covering the inner platform.

### 6.2. Intertidal shore platform versus relative sea level (RSL)

Previous studies focused on the retreat dynamics of coastal cliffs and platforms have shown that rock strength and, more generally, the physical properties of the rocks, is one of the parameters in competition with aerial and marine erosional processes like dissolution, wave impact, and freeze-thaw cycles to explain the various degrees of cliff erosion (Trenhaile, 1980, 1987; Sunamura, 1992; Duperret et al., 2002; Hénaff et al., 2002; Costa et al., 2004; Matsuoka & Murton, 2008; Young et al., 2011; Naylor & Stephenson, 2010; Prémaillon et al., 2018).

Some authors have demonstrated the impact of tidal range and wave exposure on the width and slope of shore platforms. (Trenhaile, 1978, 1987, 2002; Sunamura, 1992; Kennedy & Dickson, 2006). In Normandy, the spring tidal range is macrotidal. Astronomical tide rises progressively from Antifer (8.25 m), Fécamp (8.70 m), Le Tréport (10.05 m) to Ault (10.21 m) and wave exposition is roughly constant along the coast. The intertidal shore widths range from 120 to 435 m and the marine (inner and outer) platforms range from 280 to 810 m in width, with a mean 1.4° slope gradient. The shore platform width increases progressively from Antifer/Etretat zone (120m-170m), Fécamp/Eletot zone (215m-370m), Criel-sur-Mer/ Mesnil-Val zone (290m-435m) to Ault (300-375m). Shore platform mean slope gradients is around 1.3°, with a maximal gradient at Antifer (2.1°) and a minimal gradient at Criel sur Mer (0.8°). The width of contemporary intertidal zones tends to increase with tidal range, as well as slope gradient tend to decrease. Such tendancy is also confirmed using numeric models dedicated to RSL changes on shore platform morphology. For example, slowly rising RSL in the Bristol Channel (about 1 mm $yr^{-1}$

in the last 5000 years) created wide, gently sloping surfaces (gradients of 1° to 2° from the Mean Low Water Spring to a depth of -5m) extending from the upper intertidal zone into the subtidal zone (Trenhaile, 2010). Modelling studies suggest also that shore platform gradients may decline through time and platform width tend to increase in macro- and mesotidal runs with fast erosion (Trenhaile, 2000, 2020 ; Walkden and Hall, 2005).

### 6.3. Inner platform morphology versus chalk formations properties

In Normandy, studies based on coastal chalk cliff retreat rates have shown a direct relationship between the stratigraphy of chalk cliff outcrops and contemporary erosion rates (Costa, 1997; Costa et al., 2004; Letortu et al., 2014, 2019). It is not the case for the chalk cliffs of Sussex, where some of the spatial variability in cliff retreat rates can be explained by local variations in lithology (Dornbusch et al, 2008).

Rock strength may also explain the shape and width of the platform (Trenhaile, 1987, 1999; Stephenson & Kirk, 2000; Davies et al., 2006; Dickson, 2006). A series of 35 topo-bathymetric profiles drawn on the rock platform of each study site is superposed from the common point chosen at the $S_1$ edge location (Fig. 12). Inner platform profiles are represented according to their Chalk Formation type and location. The inner platform widths in Chalk Formations appear to vary from about 250 m to 800 m. The wider is the inner platform, the lower is its slope gradient and the higher its CPJ elevation (Fig. 12). Regardless of the Chalk Formation type, there is an apparent logarithmic relationship between the inner platform width and its slope (Fig. 13). The shortest inner platforms with high slopes are associated with the Craie de Rouen Chalk Formation and located at the Cap d'Antifer cape and the Cap Fagnet cape. The Holywell Nodular and New Pit Chalk Formations give larger inner platforms while the Lewes Nodular Chalk Formation shows the largest and flattest inner platforms, such as observed at Etretat, Eletot, Criel-sur-Mer, Mesnil-Val, and Ault (Fig. 12).

The petrophysical and geomechanical properties (porosity, permeability, Uniaxial Compressive Strength (UCS), and diagenesis index (DI)) indicative of the cementation of each chalk formation of the Paris basin have been extensively studied and measured in the laboratory (Table 1) (Mortimore & Duperret, 2004; Duperret et al., 2005; Faÿ-Gomord et al., 2016). Recently, Faÿ-Gomord et al. (2016) demonstrated the impact of chalk microtexture on its physical and mechanical properties and defined six types of chalk microtextures (MT1 to MT6) describing the texture of the chalk matrix observed using a scanning electron microscope. The widest and flattest inner platforms are shaped in the Chalk Formations that belong to the poorly to uncemented pure white chalk type (MT1) with a low UCS, a low diagenesis index, and high permeability and porosity (Lewes Nodular Chalk and New Pit Chalk Formations). The narrowest and steepest inner platforms are shaped in the Chalk Formations that largely belong to the moderately-cemented pure white chalk type (MT2) with a high UCS and diagenetic index and low permeability and porosity (Holywell Nodular Chalk and Craie de Rouen Formations).

Even if the Craie de Rouen and Holywell Nodular Chalk Formations reveal the same microtexture type (MT2), the inner platforms shaped in the Holywell Nodular Chalk Formation are mostly wider than those shaped in the Craie de Rouen Formation. This may be explained by the difference in permeability observed between these two chalk formations, where unlike the UCS, the permeability of the Craie de Rouen Formation samples is mainly lower (mean: 0.29 mD) than the samples of the Holywell Nodular Formation (mean: 0.36 mD) (Table 1). Similarly, both New Pit and Lewes Nodular Chalk Formations belong to the MT1 type but inner platforms shaped in the Lewes Nodular Chalk Formation are mainly wider. The difference in the inner platform width between the New Pit and Lewes Nodular Chalk Formations may be explained by a lower permeability for the New Pit Chalk Formation (mean: 2.4 mD) than for the Lewes Nodular Chalk Formation (mean: 10,32 mD) (Table 1).

The current width of the inner platform shows that the retreat of the cliff since it was located at the $S_1$ location is related to the lithological characteristics of chalk formations (Fig. 12). In fact, each Chalk Formation presents various geotechnical properties closely linked to its type of cementation (microtexture) and intrinsic permeability. Therefore, inner platforms shaped in the highly permeable Lewes Nodular and New Pit Chalk Formations display the largest cliff retreats, 450 to 850 m and 475 to 600 m, respectively (Fig. 12 & Fig. 13). Whereas inner platforms shaped in the lowly permeable Holywell Nodular Chalk and Craie de Rouen Formations demonstrate to the lowest cliff retreats with 325 to 440 m and 280 to 350 m, respectively (Fig. 12 & Fig. 13).

In Normandy, the higher the chalk rock permeability is, the wider and lower the slope gradient is for the inner platform.

## 7. Normandy rock platform evolution

Numerical models of shore platform evolution suggest that, whereas contemporary shore platform morphology is, in part, the product of tidal range, wave regime, rock resistance and other site-specific factors, it also reflects the way in which RSL attained its present level during the recent past (Trenhaile, 2010, Hurst et al, 2017). Holocene changes in RSL determined the amount of time that marine processes have operated within the modern intertidal zone (Tenhaile, 2010). The style of platform evolution is expected to be important for the distribution of $^{10}$Be across the shore platform (Regard et al, 2012, Hurst et al, 2016, 2017). Dynamic shore profile evolution models (e.g. Sunamura, 1992; Anderson et al, 1999; Trenhaile, 2000; Walkden and Hall, 2005; Matsumoto et al, 2016) predict that coasts tend towards steady state, whereby rapid cliff retreat widens shore platforms and the resultant increased wave energy dissipation reduces cliff retreat rates and increases erosion of the shore platform (Hurst et al, 2017).

The $^{10}$Be production on a shore platform formed during the Holocene is a progressive increase of $^{10}$Be concentration from the nearshore zone to offshore because the shore platform has been exposed for longer. However, the rate of $^{10}$Be production decreases offshore because cover by seawater attenuates the cosmic ray flux; hence, the amount of cosmic radiation received by the platform decreases with increased water depth. The combined result of these factors is a “humped” distribution of $^{10}$Be concentrations. The magnitude of the maximum concentration is predicted to be inversely proportional to the rate of cliff retreat (Regard et al, 2012; Hurst et al, 2016, 2017).

### 7.1. $^{10}$Be concentration pattern

In Mesnil-Val, six new samples (MEV1 to MEV6) were collected between 456 and 814 m from the cliff in order to complement the eight samples (MV01 to MV08) from Regard et al. (2012) (Fig. 14 & Table 2). These new flint samples were collected and georeferenced by divers beyond the shore platform limit (LAT), in the subtidal portion of the rock platform. In addition, nine new samples were collected from the Senneville-sur-Fécamp shore platform (SEN1 to SEN9) (Fig. 14). They are only located in the intertidal area close to the cliff and range from 125 m to 239 m from the cliff (Fig. 14 & Table 3). The SEN1 to SEN3 samples were initially collected and analysed in 2007, followed by the SEN6 to SEN9 samples in 2015 (Fig. 15). All samples have been prepared following a standard procedure (e.g.

Regard et al., 2012).

In Mesnil-Val, despite the samples having been collected at a distance of 600 m away from the cliff face, Regard et al (2012) did not find the expected signature of the glacial cliff position, characterized in the model by a step toward higher concentrations offshore. The model fit led Regard et al (2012) to the conclusion that cliff retreat rate integrated over 6000 years cannot be lower than 10 cm/yr. As model evaluation is very sensitive to the assumed rate of recent sea level rise, a retreat rate of 11-13 cm/y over the last 3 ky was finally proposed (Regard et al, 2012).

The new sampling extends as far as 800 m away from the cliff face and shows a characteristic “humped” shape (Fig. 14), as initially expected. Here, we observed a marked step in $^{10}$Be concentrations between MEV2 (2.5 kat/g), and MEV3 (17.9 kat/g) along the same transect (Fig. 14). Most of the samples of the Muron rocks inner platform (MEV3, MEV4b, MEV1 and MEV6) show an increased $^{10}$Be concentration of ten to fourteen times higher than the MV01 to MV07 samples collected on the shore platform. The closer the sample is to $S_1$, the higher its $^{10}$Be concentration is. The MEV3 concentration correlates with the morphological $S_1$ step and corresponds (in position and magnitude of the concentration step) to the last glacial cliff position expected by Regard et al. (2012). The highest $^{10}$Be concentration is for MEV6 (46.3 kat/g) localised nearby $S_1$, and locally close to LAT (Fig. 14). Such a high $^{10}$Be concentration may result from a long long presence of the glacial cliff at this location, amplified by a lack of shielding due to the absence of beach cover and glacial chalk cliff slope degradation.

The Senneville-sur-Fécamp shore platform is short and roughly flat (<1.3°) and all SEN samples are collected in the 1 to 1.5m thick Hardground band, with flints called Tilleul’s hardgrounds (HG1-2) corresponding to the lithological transition between the Holywell Nodular and overlying Newpit Chalk Formations (Mortimore et al., 2001) (Fig. 6). The HG1-2 band testifies to the hardness of this layer in comparison to the underneath located chalk (Holywell Nodular Chalk Formation) that constitutes the shore platform. At Senneville-sur-Fécamp, the samples that have been collected closest to the cliff (SEN1 to SEN3) have $^{10}$Be concentrations that are similar to most of the Mesnil-Val shore platform samples (MV01 to MV08), with the exceptions of MEV4a/4b (Table 3). The distal shore platform samples (SEN5 to SEN9) show a three to five fold enhanced $^{10}$Be concentrations three to five times higher than the SEN1 to SEN3 and MV samples located close to the cliff in the proximal shore platform (Fig. 14 &15). The $^{10}Be$ enrichment of the distal shore platform was also observed in Sussex, UK (Hurst et al, 2016) and in Yorkshire, UK (Swirad et al, 2020), at a distance of about 200 m to 300 m from the cliff face, respectively. Unfortunately, the small number of samples collected from the Senneville sur Fécamp shore platform is insufficiant to provide values of apparent exposure ages deduced from cosmic radiations. The SEN6 to SEN8 concentrations are quite similar to those of MEV3, but unlike the Mesnil-Val site such concentrations do not testify to the last glacial cliff position ($S_1$) located offshore (Fig. 15).

**7.2. Evolution of the cliff/platform system**

At Mesnil-Val, $S_1$ is located 180 m farther than the Muron Rocks. $S_1$ is thus older than the Muron Rocks whose exposure age is evaluated from $^{10}Be$ concentrations (MV1 to MV7 samples) as being between 4.6-5.4 kyr BP (Regard et al., 2012). If the cliff retreat rate has not changed, $S_1$ could be 5.9 to 6.9 kyr old.

At 6.5 ky ± 1 ky BP, the Holocene sea level rise slowdown is identified at different places around the world, dated from coral reefs in Barbados (Fairbanks, 1989), from melting ice sheet and isostatic models in Western Europe (Lambeck, 1997; Shennan et al., 2012), from $^{14}C$ dating on foraminifera in England and the British Isles (Horton & Edwards, 2005; Massey et al., 2008), and from $^{14}C$ dating of sediments infilling in the Seine estuary (Frouin et al., 2007; Tessier et al., 2012). In Normandy, high-resolution seismic profiles acquired in the sedimentary infill of the Seine estuary, southwest of Le Havre, show an architectural change of marine deposits symbolised by Transgressive Systems Tracts corresponding to a quick sea level rise (10 mm/y), a Maximum Flood Surface and Highstand System Tract corresponding to a slow sea level rise (1-3 mm/yr) (Lambeck, 1997). Using $^{14}C$ dating, the Maximum Flood Surface located at -9 m (NGF) on the Seine Estuary channel edges and at -13 m (NGF) in the Seine channel axis was dated at around 6.5 ky BP (Tessier et al., 2012).

Moreover, at 20 km north of Mesnil-Val, some peat layers were discovered in two boreholes made north of Ault, in the lowland of “Bas-Champs de Cayeux”, where the cliff-line disappears gradually inland. Sedimentary infill covers the chalk rock platform and peat layers are interspersed with grey silt.

Peats recognised between -10 m to -6 m (NGF) are dated from 5.5 ky to 7.5 ky BP (Beun & Broquet, 1980). Buried peat layers attest to the sea-level rise slowing down during the Mid-to Late Holocene.

When compared, the observed depth of $S_1$ in the chalk resulting from an erosive process and the depth of sediment accumulation in the Seine estuary and Cayeux lowland are quite equivalent. Taking into account the current depth of S1 (top) at -10m, we suggest that the formation of $S_1$ occurred during the Holocene sea level rise slowdown at 6.5 ky ± 1 ky BP.

We have taken into account that the $S_1$ edge remained static and the widening of the platform over time is only the product of cliff retreat processes (Johnson, 1919; de Lange & Moon, 2005; Walkden & Hall, 2005), following a static evolution model (Sunamura, 1983; Trenhaile, 2000, 2001a, 2001b; de Lange & Moon, 2005). Therefore, $S_1$ is a submarine geomorphological feature indicative of the paleo-cliff location during a past sea level slowdown at about 6.5 ky ± 1 ky BP. We thus consider the location of the present-day cliff-line as an onshore translation of the $S_1$ edge using a constant cliff retreat rate through the Holocene, which creates the inner shore platform (Fig. 16). The cliff previously located on $S_1$ is a fossil remnant of the active cliff during the previous highstand sea level, the MIS5e (125 ky BP, Siddall et al., 2007) that underwent degradation by subaerial periglacial processes during the last glacial periods (MIS4 to MIS2), when the sea was far away.

The outer platform edge, $S_2$, is found at -17m (NGF) offshore the Cap d'Antifer cape and in the Biville-sur-Mer section where it is partially covered with sand. $S_2$ is not found in the other studied sections due to the gravel cover offshore Fécamp, Senneville-sur-Fécamp, Criel sur-Mer, Mesnil-Val, and Ault.

The outer platform, extending spatially 500m wide, from depths of -17m (top of S2) to about -15m (base of S1) is associated with a sea-level stillstand necessarily lower than the Holocene sea level rise responsible for the inner platform creation.

A similar subtidal cliff is also reported along the submarine rock platform of the NW Cotentin (NW Normandy located in the North Armorican massif), at about -20 m depth, where it is associated with past sea level stillstands estimated at MIS5a and/or MIS5c (Coutard et al., 2006), when the sea level was lower than during MIS5e. Based on a similar depth, we assume the same origin for the $S_2$ edge observed offshore the Cap d'Antifer cape at -17 m and the subtidal cliff of NW Cotentin observed at -

20 m, as a shoreline angle track of the previous high sea level of MIS 5a and/or 5c, dated at 96 and/or 82 ky (Fig. 16).

As observed along the northern Iberian Peninsula in the Bay of Biscay, a sequence of twelve submerged marine terraces were identified at various depths, ranging from -13m to -92m. They illustrate the irregularity of the preservation of fossil shorelines preservation and submerged submarine terraces that seem to depend on the interplay between wave climatology, lithology, and bedding direction (Bilbao-Lasa et al, 2020). The preservation of the outer platform and its edge (S2) offshore the Cap d'Antifer cape may impact the lithological change of the underlying Gaize Formation to the overlying Glauconitic Chalk Formation (Fig. 4). Some relicts of Pleistocene raised beaches are still preserved on the English Channel coast in England (Black Rock, Brighton marina) (Smith, 1936, Mortimore, 1997, Parfitt et al., 1998) and in Sangatte, France (Sommé et al., 1999, Antoine et al., 2011). They are evidence of Pleistocene shore platforms sealed with "head" deposits formed as scree, solifluction, and hillslope wash sediments that flow over the ancient chalk cliff line during wetter and periglacial climates. During the last glacial period, the outer platform probably created during the MIS5e highstand sea-level was sealed under periglacial deposits, and only recently rejuvenated following the Holocene marine transgression (Fig.16).

### 7.3. Long-term retreat rates on Normandy chalk cliffs

#### 7.3.1. Contemporary cliff retreat

Contemporary retreat rates have been estimated along 50 m bins along the coast stretch by aerial photogrammetric analysis of the cliff top between 1966 and 1995 (Costa et al., 2004), and 1966-2008 (Letortu et al., 2014). The coastal section from the Cap d'Antifer cape to Etretat shows the lowest retreat rates with a mean of 0.088 m/y. Between Fécamp and Eletot, the mean retreat rate is 0.118 m/y, with local high retreat rates that are sometimes greater than 0.5 m/y. Finally, the section between Biville-sur-Mer and Mesnil-Val shows the highest contemporary mean retreat rate of 0.135 m/y (Costa et al., 2004; Letortu et al., 2014) (Fig. 17).

#### 7.3.2. Long-term (Holocene) cliff retreat

Cosmogenic nuclides ($^{10}Be$) in Mesnil-Val and Senneville-sur-Fécamp, indicate that $S_1$ dates back to about 6ka BP. Regional correlations indicate that this date corresponds to the sea level rise up to its current level, and the ensuing reactivation of coastal erosion and cliff retreat. A compilation of data from $^{10}Be$ and from literature led us to estimate this episode at 6.5 ± 1 ky BP.

The total Holocene cliff retreat rate is calculated using the distance between the paleo-cliff ($S_1$) and the current cliff location. Using a duration of 6.5 ± 1 ky, long-term average retreat rates are calculated and compared to the contemporary ones (Fig. 17). The Ault long-term retreat rates could not be calculated due to the lack of $S_1$ edge observations. Unlike contemporary retreat rates, long-term retreat rates (6.5 ky) are spatially quite homogenous. This is due to the constant distance between $S_1$ and the current coastline. Some rocky capes behave differently, like between le Tilleul and Etretat, where the long-term retreat rate is lower than the current one (*Manneporte* and *Porte d'Aval*) (Fig. 17). Along the section from the Cap d'Antifer cape to Etretat the long-term average cliff retreat rate is 0.051 m/y ± 0.008 m/y. This represents the lowest rate observed along the studied coastal sections. Between Fécamp and Eletot, the long-term mean retreat rate is 0.060 m/y ± 0.009 m/y with a slight increase between Fécamp and Eletot in the case of contemporary retreat rates (Fig. 17). From Biville-sur-Mer to Mesnil-Val the long-term average cliff retreat rate of 0.090 m/y ± 0.014 m/y is the highest one observed. At Mesnil-Val, where the inner platform is the widest, at the Muron rocks, the long-term retreat rate is 0.13 m/y ± 0.014 m/y, which is quite similar to the retreat values estimated on the shore platform by Regard et al. (2012) using cosmogenic dating (0.11- 0.13 m/y) (Fig. 17).

Long-term mean retreat rates calculated over the period from 6.5 ky ± 1ky BP to today are 33% (Biville to Mesnil-Val section) to 57% (Fécamp to Eletot section) slower than the corresponding contemporary cliff retreat rates, suggesting a recent acceleration in the erosion of coastal chalk cliff sections, as has also been observed on the south coast of Great Britain (Hurst et al., 2016).

## 7. Conclusion

The new high resolution topo-bathymetric DEMs generated for the Normandy chalky coast show a submarine rocky platform composed of a continuous inner platform and local outer platform. One study site offshore the Cap d'Antifer cape illustrates the occurrence of an outer platform delineated by a step ($S_2$) located at -17 m. Analogous to the submarine cliffs reported in the crystalline geological framework of western Normandy, we assume that such a deep platform could be associated to an old high sea level stillstands dating from MIS5a and/or MIS5c (96 and 82 ky BP, respectively). We demonstrated that the inner platform edge ($S_1$), located at -9 m to -10 m (NGF), can be associated with the previous position of the cliff, corresponding to the cliff position before the sea level dropped at the end of the last glacial period (MIS2). Therefore, the Normandy inner platform developed since the Holocene and gradually widened through cliff retreat and downwearing. The inner platform width is a direct function of the chalk lithology characteristics and the tidal regime. The higher the intrinsic permeability of the chalk and the higher the tidal regime are, the wider the platform is.The 10Be cosmogenic concentration of shore and inner platform samples allowed estimating the starting moment of the current cliff retreat to be 6.5 ± 1 ky BP. This moment corresponds to the slowing down of the Holocene sea level rise. Finally, we calculated the average Normandy cliff retreat rates since 6.5 ky ± 1 ky using the distance between $S_1$ and the current cliff line. Cliff retreat rates since 6.5 ky ± 1 ky varied from 0.051 m/y ± 0.008 m/y to 0.090 m/y ± 0.014 m/y, lower by 33% to 57% while compared to the contemporary ones for each study site. This result suggests an acceleration of coastal cliff retreats rates in Normandy during the contemporary period.

## Acknowledgments

This work is part of a PhD thesis (T.D) and received a grant awarded by Le Havre Normandie Université allocation. The INSU/CNRS French national program EC2CO (Ecosphère Continentale et Côtière) - DRIL (CROCO-DYL project) supported this work. Data used to merge detailed onshore-offshore DEMs was provided from the French National Institute of Geography (IGN) for the BDALTI25 and the RGEALTI databases. Some LIDAR data surveyed by the CIRCLE crew from UMR 6143 M2C (Université Caen Normandie) were used on the Mesnil-Val site and a TLS DEM for Senneville-sur-Fécamp was part of the INSU-CNRS RELIEF (2007) project conducted by V.R. The CROCOLIT-2013, SPLASHALIOT-2014, and CROCO-CAUX-2017 cruises were operated on the R/V Haliotis (IFREMER) and we would like to thank the CNFC and the Haliotis's crew (Genavir) for their work. Finally, the Normandy Region sustained project RIN SELINE allowed to us to perform cosmogenic measurements at the ASTER AMS national facility, CEREGE (Aix-en-Provence) under the supervision of Regis Braucher and Laetitia Leani. We are also grateful to the Editor Edward Anthony and the reviewers (Brian Finlayson and two others anonymous reviewers) whose suggestions undoubtely contributed to improve our article.

## Table Captions

**Table 1**: Petrophysical and geomechanical properties of the Normandy, Hauts de France, and Sussex chalk samples with: D.I (diagenesis index), $\phi$ (porosity), K (permeability), and UCS (uniaxial compressive strength). [1] Duperret et al. 2005, [2] Faÿ-Gomord et al, 2016.

**Table 2**: Sample $^{10}Be$ concentrations and uncertainty measured on *in situ* flint samples at the Mesnil-Val rock platform. MV samples are from the shore platform (Regard et al., 2012). MEV are the new subtidal samples from the rock platform (this study).

**Table 3**: $^{10}Be$ concentrations and uncertainty measured on *in situ* flint samples at the Senneville-sur-Fécamp shore platform.

## Figure Captions

**Figure 1**: Geological map of eastern coastal Normandy (adapted from Duperret et al., 2012). (A) DEM map with Normandy geology corresponding to the west border of the Paris basin (Neau, 1979). Rose diagram represents main wave orientations recorded at the Penly buoy from January 2018 to March 2019 (CEREMA, 2018). Localisation of CROCOLIT, SPLASHALIOT, and CROCOCAUX cruise (R/V Haliotis) navigation tracks. Black squares refer to detailed figures of the manuscript. (B) Geological cliff section from the Cap d'Antifer cape to Ault, covering a distance of 140 km and showing cliff face exposure from 20 to 120 m high, with a vertical exaggeration of 100. Abbreviations of the geological section are FQ: Le Fourquet, FC: Fécamp, SF: Senneville-sur-Fécamp, SVC: Saint Valéry en Caux, F-L fault: Fécamp-Lillebonne fault, and M/V: Mesnil-Val.

**Figure 2**: Stratigraphy and lithostratigraphy of the Chalk Formations, with field key-markers in Normandy, adapted from Mortimore (2001); Duperret et al.(2012) and Lower Cretaceous Formations reported from the field (Juignet (1974) and local boreholes (BRGM database)).

**Figure 3**: (A) Land-sea DEM of the the Cap d'Antifer cape to Etretat coastal section with bathymetric cover. The colour-scale is indicative of depth, with variations from +20m to -20m. Detailed bathymetry

is provided by the CROCAUX cruise and the land DEM from RGEAlti (IGN). Continuous black line corresponds to the Low Astronomical Tide Level (LAT) located at -4.2 m (NGF). White lines correspond to morphological steps/edges ($S_0$, $S_1$, and $S_2$) (see text). (B) Detail of the land-sea DEM of the shore and subtidal rock platforms at Le Fourquet. Black lines are isobaths labeled in meters. (C) 3D view from the west of the bathymetric dataset between Etretat and Le Tilleul, illustrating steps of the subtidal rock platform, with high vertical exaggeration.

**Figure 4**: (A) Offshore lithological map of the the Cap d'Antifer cape to Etretat section. White lines correspond to morphological steps/edges ($S_0$, $S_1$, and $S_2$). Dip symbols refer to field observations. Red stars are the location of the geological boreholes made by the BRGM at Le Tilleul and Etretat (1963, 1970). (B) Topo-bathymetric profile of the rock platform, with vertical exaggeration (V.E.=12) based on the national terrestrial reference origin (NGF). Outcrop lithologies (Chalk Formations) are interpreted from field observations on the cliff face and the shore platform. CPJ is the Cliff Platform Junction located at 0.5 m high (NGF). The surface between the High Astronomical Tide (HAT) and the Low Astronomical Tide (LAT) correspond to the intertidal domain. HAT is at 4.64 m (NGF) and LAT at -4.2 m (NGF).

**Figure 5**: (A) Land-sea DEM of the Fécamp to Eletot coastal section with bathymetric cover. Detailed bathymetry is provided by the CROCOCAUX cruise and land DEM from RGEAlti (IGN). The color-scale is indicative of the depth, with variations from +20m to -20m. Solid black line corresponds to the Low Astronomical Tide Level (LAT) at -4.2 m (NGF). White lines correspond to morphological steps/edges ($S_0$ and $S_1$). A bathymetric detail shows a large paleo-scree indenting the $S_1$ step offshore Senneville-sur-Fécamp (see text). (B) Detailed Land-sea DEM of the shore and subtidal rock platforms at the Cap Fagnet cape. Black lines are isobaths labeled in meters. (C) 3D view from the NW of the bathymetric dataset between Eletot and Senneville-sur-Fécamp illustrating steps of the subtidal rock platform, with high vertical exaggeration.

**Figure 6**: (A) Offshore lithological map of the Fécamp to Eletot section. White lines correspond to morphological steps/edges ($S_0$ and $S_1$). Dip symbols refer to field observations. Red star is the location of the geological borehole conducted by the BRGM (1969) at Fécamp. (B) Topo-bathymetric profile of the rock platform, with vertical exaggeration (V.E.=12) based on the national terrestrial reference origin (NGF). Outcrop lithologies (Chalk Formations) are interpreted from field observations

on the cliff face and the shore platform. CPJ is the Cliff Platform Junction located at about 2 m high (NGF). The surface between the High Astronomical Tide (HAT) and the Low Astronomical Tide (LAT) corresponds to the intertidal domain. HAT is located at 4.64 m (NGF) and LAT at -4.2 m (NGF).

**Figure 7**: (A) Land-sea DEM of the Biville-sur-Mer to Mesnil-Val (MV) coastal section with bathymetric cover. Detailed bathymetry is provided by the CROCOLIT-1 and SPLASHALIOT-02 cruises and land DEM from RGEAlti (IGN). The color-scale is indicative of the depth, with variations from +20m to -20m. Continuous black line corresponds to the Low Astronomical Tide Level (LAT) at -4.4 m (NGF). White lines correspond to morphological steps/edges ($S_0$ and $S_1$). Abbreviation of the map is MV: Mesnil-Val. (B) Detailed Land-sea DEM of the shore and subtidal rock platforms at Criel-sur-Mer. Black lines are isobaths labeled in meters. (C) 3D view from the NW of the bathymetric dataset west of Criel-sur-Mer side illustrating steps of the subtidal rock platform, with high vertical exaggeration.

**Figure 8**: (A) Offshore lithological map of Biville-sur-Mer to Mesnil-Val (MV) section. Dip symbols refer to field observations. White lines correspond to morphological steps/edges ($S_0$ and $S_1$). Red star is the location of the geological borehole made by the BRGM (1956) at Criel-sur-Mer. Abbreviation of the map is MV: Mesnil-Val. (B) Topo-bathymetric profile of the rock platform, with vertical exaggeration (V.E.=12) based on the national terrestrial reference origin (NGF). Outcrop lithologies (Chalk Formations) are interpreted from field observations on the cliff face and the shore platform. CPJ is the Cliff Platform Junction located at about 2 m high (NGF), referring to the national terrestrial reference origin (NGF). The surface between High Astronomical tide (HAT) and the Low Astronomical Tide (LAT) corresponds to the intertidal domain. HAT is at 5.8 m (NGF) and LAT at -4.4 (NGF).

**Figure 9**: Bathymetry and one Chirp profile "Splash33" (from SPLASHALIOT-02 cruise) and reference boreholes (BRGM-5 and BRGM-6) with stratigraphical interpretations (BRGM, 1993) located offshore Penly at 3.8 km SW from Criel-sur-Mer, illustrating the $S_1$ continuity along the coast (white line) and the outer platform surface of the rock platform located under Pleistocene sands.

**Figure 10**: (A) Land-sea DEM of the Ault coastal section with the bathymetric cover of CROCOLIT-01 cruise. The solid black line corresponds to the Low Astronomical Tide Level (LAT) at -4.4 m (NGF). (B) Land-sea DEM of the shore platform at the Second-Val location. The solid black line corresponds to the Low Astronomical Tide Level (LAT) -4.4 m (NGF). Black lines are isobaths labeled in meters. (C) Offshore DEM of the elevation of the chalk basement generated from seismic profile interpretations

(CROCOLIT_01, 2013). White line corresponds to the edge $S_1$. (D) Offshore lithological map of the Ault section with sand isopachs (m). Black line corresponds to the inner platform edge ($S_1$) located under the sand cover. Red star is the location of the BRGM-7 geological borehole made by the BRGM (1973).

**Figure 11**: 3D conceptual model of the chalk cliff/rock platform system in Normandy. CPJ is the Cliff Platform Junction. $S_2$ is the rock platform edge, $S_1$ is the edge that delineates the inner platform and the outer platform, and $S_0$ is a step corresponding to a hardground or a lithological transition. Altitudes and depths of each slope rupture are indicated, referred to the NGF system. LAT and HAT are the Low Astronomical Tide and the High Astronomical Tide levels, respectively.

**Figure 12**: Graph representing 35 rock platform topo-bathymetric profiles drawn on the four coastal sections studied with the inner platform edge ($S_1$) considered as common point. Each color refers to a Chalk Formation unit and the symbols to the location along the coast.

**Figure 13**: Chalk inner platform slopes (in degree) versus inner platform width (in meters), as a function of the Chalk Formation, performed on 45 random bathymetry profiles along the four study sites detailed in this manuscript. Colors and symbols refer to a Chalk Formation unit.

**Figure 14**: A. Detailed DEMs of the Senneville-sur-Fécamp shore and rock platform (CROCOCAUX cruise). Flint samples location (SEN) on the shore platform is shown. The solid black line corresponds to the level of astronomical tide (LAT) and delineates intertidal shore platform and subtidal rock platform. $S_1$ location is indicated. B. $^{10}$Be sample concentrations and error bars versus the distance of the sample from the cliff (CPJ).

**Figure 15**: A. Detailed DEMs of the Mesnil-Val shore and rock platform (CROCOLIT-1 cruise). Flint samples location (MV) on the shore platform is from Regard et al. (2012). MEV samples are new and collected by divers on the subtidal rock platform. The solid black line corresponds to the level of astronomical tide (LAT) and delineates intertidal shore platform and subtidal rock platform. $S_1$ location is indicated and locally limits the Muron rocks subtidal plateau. B. $^{10}$Be sample concentrations and error bars versus the distance of samples from the cliff (CPJ).

**Figure 16**: Conceptual 3D block diagram evolution model of the Normandy Chalk cliff/rockplatform system depending on Holocene and Late Pleistocene sea-level variations and derived from the current

conceptual morphology of the coast. The past sea-level variation curve is adapted from Lambeck (1997). Each block diagram represents a past situation of the system. a: present-day, b: 4kyr, c: 6.5 kyr, d: Between MIS2 and MIS4, e: between MIS5a and MIS 5c, f: MIS5e. See explanations in the text.

**Figure 17**: Comparison of modern cliff retreat rates in grey (Costa et al., 2004; Letortu et al., 2014), 3 ky retreat rates at Mesnil-Val ($^{10}Be$ dating, Regard et al., 2012) indicated with a triangle and long term retreat rates (this study, 6.5 ky ± 1 ky) in black, measured from the inner platform edge ($S_1$) to the present day cliff position of three coastal sections: the Cap d'Antifer cape to Etretat, Fécamp to Eletot, and Biville-sur-Mer to Mesnil-Val.

## References


Amédro, F., & Robaszynski, F., 2000. Les craies à silex du Turonien supérieur au Santonien du Boulonnais (France) au regard de la stratigraphie événementielle. *Géologie de France*, *4*, 39-56.

Anderson R.S., Densmore A.L., Ellis M.A., 1999, The generation and degradation of marine terraces, *Basin Research*, 11, 7-19.

Antoine P., Auguste P., Bahain J.J., Longuet S., 2011, Datation et reconstruction paléoenvironnementale d'un site paléolithique moyen submergé en Manche Est : Ault-Onival (Somme, France), Quaternaire, vol 22/3, 221-233.

Augris, C., Clabaut, P., Bourillet, J., Dréves, L., 1993. Carte morpho-sédimentaire du domaine côtier entre Dieppe et Le Tréport (Seine-Maritime). Notice explicative. IFREMER

Augris, C., Clabaut P. Costa S., Latteux B., Gourmelon F., 2004. *Evolution morpho-sédimentaire du domaine littoral et marin de la Seine-Maritime*. Editions Quae.

Beun & Broquet, 1980. Tectonique quaternaire (Holocène ?) dans la plaine littorale picarde des « Bas-Champs de Cayeux » et de leurs abords orientaux. In : Bulletin de l'Association française pour l'étude du quaternaire – Volume 17- Numéro 1-2. Pp. 47-52.

Bilbao-Lasa P., Jara-Munoz J., Pedoja K., Alvarez I., Aranburu A., Iriarte E., Galparsoro I, 2020, Submerged marine terraces identification and an approach for numerical modeling the sequence formation in the Bay of Biscay (Northeastern Iberian Peninsula), Frontiers in Earth Science, 8, 47.

Blanco Chao, R., Costa Casais, M., Martínez Cortizas, A., Pérez Alberti, A., Trenhaile, A. S., 2003. Evolution and inheritance of a rock coast: western Galicia, northwestern Spain. *Earth Surface Processes and Landforms: The Journal of the British Geomorphological Research Group*, *28*(7), 757-775.

BRGM, 1956. Banque du sous-sol, BSS000DTWM, Criel-sur-Mer (76192). http://ficheinfoterre.brgm.fr/InfoterreFiche/ficheBss.action?id=BSS000DTWM.

BRGM, 1963. Banque du sous-sol, BSS000EKFG, Etretat (76254). http://ficheinfoterre.brgm.fr/InfoterreFiche/ficheBss.action?id=BSS000EKFG.

BRGM, 1969. Banque du sous-sol, BSS000ELDU, Fécamp (76259). http://ficheinfoterre.brgm.fr/InfoterreFiche/ficheBss.action?id=BSS000ELDU.

BRGM, 1970. Banque du sous-sol, BSS000EKHC, Le Tilleul (76693). http://ficheinfoterre.brgm.fr/InfoterreFiche/ficheBss.action?id=BSS000EKHC.

BRGM, 1973. Banque du sous-sol, BSS000DDQB, Woignarue (80826). http://ficheinfoterre.brgm.fr/InfoterreFiche/ficheBss.action?id=BSS000DDQB.

BRGM, 1993. Banque du sous-sol, BSS000DTWB/ BSS000DTWD, Penly (76618).http://ficheinfoterre.brgm.fr/InfoterreFiche/ficheBss.action?id=BSS000DTWB http://ficheinfoterre.brgm.fr/InfoterreFiche/ficheBss.action?id=BSS000DTWD

Brossard, J., & Duperret, A., 2004. Coastal chalk cliff erosion: experimental investigation on the role of marine factors. *Geological Society, London, Engineering Geology Special Publications*, *20*(1), 109-120.

Castleden, R., & Green, C., 1996. *Classic landforms of the Sussex coast*. Sheffield: Geographical Association.

CEREMA, 2019. http://candhis.cetmef.developpement-durable.gouv.fr/

Choi, K. H., Seong, Y. B., Jung, P. M., Lee, S. Y., 2012. Using cosmogenic 10Be dating to unravel the antiquity of a rocky shore platform on the west coast of Korea. *Journal of Coastal Research*, *28* (3), 641-657.

Costa, S., 1997. Dynamique littorale et risques naturels : L'impact des aménagements, des variations du niveau marin et des modifications climatiques entre la Baie de Seine et la Baie de Somme. Thèse de doctorat, Université de Paris I.

Costa, S., Delahaye, D., Freiré-Diaz, S., Di Nocera, L., Davidson, R., Plessis, E., 2004. Quantification of the Normandy and Picardy chalk cliff retreat by photogrammetric analysis. *in*: Mortimore R.N. and Duperret A. (eds), *Coastal Chalk Cliff instability*. Geological Society, London, Engineering Geology Special Publications, 20 (1), 139-148.

Costa, S., Laignel, B., Hauchard, E., Delahaye, D., 2006. Facteurs de répartition des entonnoirs de dissolution dans les craies du littoral du Nord-Ouest du Bassin de Paris. *Zeitschrift für Geomorphologie, NF*, 95-116.

Coutard, S., Lautridou, J. P., Rhodes, E., Clet, M., 2006. Tectonic, eustatic and climatic significance of raised beaches of Val de Saire, Cotentin, Normandy, France. *Quaternary Science Reviews*, *25* (5-6), 595-611.

de Lange, W. P., & Moon, V. G., 2005. Estimating long-term cliff recession rates from shore platform widths. *Engineering Geology*, *80* (3-4), 292-301.

Davies, P., Sunamura, T., Takeda, I., Tsujimoto, H., & Williams, A. T., 2006. Controls of shore platform width: the role of rock resistance factors at selected sites in Japan and Wales, UK. *Journal of Coastal Research*, 160-164.

Dewez, T. J., Rohmer, J., Regard, V., Cnudde, C., 2013. Probabilistic coastal cliff collapse hazard from repeated terrestrial laser surveys: case study from Mesnil Val (Normandy, northern France). *Journal of Coastal Research*, *65* (sp1), 702-707.

Dewez, T. J. B., Regard, V., Duperret, A., Lasseur, E., 2015. Shore platform lowering due to frost shattering during the 2009 winter at mesnil Val, English Channel coast, NW France. *Earth Surface Processes and Landforms*, *40*(12), 1688-1700.

Dickson, M. E., 2006. Shore platform development around Lord Howe Island, southwest Pacific. *Geomorphology*, *76*(3-4), 295-315.

Dornbusch, U., Robinson, D. A., Moses, C., Williams, R., Costa, S., 2006. Retreat of Chalk cliffs in the eastern English Channel during the last century. *Journal of Maps*, *2* (1), 71-78.

Dornbusch, U., Robinson, D. A., Moses, C. A., Williams, R. B., 2008. Temporal and spatial variations of chalk cliff retreat in East Sussex, 1873 to 2001. *Marine Geology*, *249* (3-4), 271-282.

Dornbusch, U., & Robinson, D. A., 2011. Block removal and step backwearing as erosion processes on rock shore platforms: a preliminary case study of the chalk shore platforms of south-east England. *Earth Surface Processes and Landforms*, *36*(5), 661-671.

Dunai, T. J., 2010. *Cosmogenic Nuclides: Principles, concepts and applications in the Earth surface sciences*. Cambridge University Press.

Duperret, A., 2013a. CROCOLIT_LEG1 cruise, RV Haliotis, http://dx.doi.org/10.17600/13120080

Duperret, A., 2013b. CROCOLIT_LEG3 cruise, RV Haliotis, http://dx.doi.org/10.17600/13120100

Duperret, A., 2017. CROCO-CAUX cruise, RV Haliotis, https://doi.org/10.17600/17008200

Duperret, A., Genter, A., Mortimore, R. N., Delacourt, B., De Pomerai, M. R., 2002. Coastal rock cliff erosion by collapse at Puys, France: the role of impervious marl seams within chalk of NW Europe. *Journal of Coastal Research*, 52-61.

Duperret, A., Genter, A., Martinez, A., Mortimore, R. N., 2004. Coastal chalk cliff instability in NW France: role olithology, fracture pattern and rainfall. *in*: Mortimore R.N. and Duperret A. (eds), *Coastal Chalk Cliff instability*. Geological Society, London, Engineering Geology Special Publications, 20 (1), 33-55.

Duperret, A., Taibi, S., Mortimore, R. N., Daigneault, M., 2005. Effect of groundwater and sea weathering cycles on the strength of chalk rock from unstable coastal cliffs of NW France. *Engineering Geology*, *78* (3-4), 321-343.

Duperret, A., Vandycke, S., Mortimore, R. N., Genter, A., 2012. How plate tectonics is recorded in chalk deposits along the eastern English Channel in Normandy (France) and Sussex (UK). *Tectonophysics*, *581*, 163-181.

Duperret, A., Raimbault, C., Le Gall, B., Authemayou, C., van Vliet-Lanoë, B., Regard, V., Dromelet, E., Vandycke, S., 2016. High-resolution onshore–offshore morpho-bathymetric records of modern chalk and granitic shore platforms in NW France. *Comptes Rendus Geoscience*, *348* (6), 422-431.

Fairbanks, R. G., 1989. A 17,000-year glacio-eustatic sea level record: influence of glacial melting rates on the Younger Dryas event and deep-ocean circulation. *Nature*, *342*(6250), 637.

Faÿ-Gomord, O., Descamps, F., Tshibangu, J. P., Vandycke, S., Swennen, R., 2016. Unraveling chalk microtextural properties from indentation tests. *Engineering Geology*, *209*, 30-43.

Foote, Y., Plessis, E., Robinson, D. A., Henaff, A., Costa, S., 2006. Rates and patterns of downwearing of chalk shore platforms of the Channel Coasts: comparisons between France and England. *Zeitschrift fur Geomorphologie Supplementband*, *144*, 93-115.

Frouin, M., Sebag, D., Durand, A., Laignel, B., Saliege, J. F., Mahler, B. J., & Fauchard, C., 2007. Influence of paleotopography, base level and sedimentation rate on estuarine system response to the Holocene sea-level rise: the example of the Marais Vernier, Seine estuary, France. *Sedimentary Geology*, *200*(1-2), 15-29.

Gosse, J. C., & Phillips, F. M., 2001. Terrestrial in situ cosmogenic nuclides: theory and application. *Quaternary Science Reviews*, *20*(14), 1475-1560.

Haslett, S. K., & Curr, R. H., 2001. Stratigraphy and palaeoenvironmental development of Quaternary coarse clastic beach deposits at Plage de Mezpeurleuch, Brittany (France). *Geological Journal*, *36*(2), 171-182.

Hauchard, E., & Laignel, B., 2008. Morphotectonic evolution of the north-western margin of the Paris Basin. *Zeitschrift für Geomorphologie*, *52* (4), 463-488.

Hénaff, A., Lageat, Y., Costa, S., Plessis, E., 2002. Le recul des falaises crayeuses du Pays de Caux: détermination des processus d'érosion et quantification des rythmes d'évolution/Retreat of chalk cliffs in the Pays de Caux: processes and rates. *Géomorphologie: relief, processus, environnement*, *8*(2), 107-118.

Hénaff, A., Lageat, Y., Costa, S., 2006. Geomorphology and shapping processes of chalk shore platforms of the Channel coasts. *Annales de Géomorphologie/Annals of Geomorphology/Zeitschrift für Geomorphologie*, *144*, 61-91.

Horton, B. P., & Edwards, R. J., 2005. The application of local and regional transfer functions to the reconstruction of Holocene sea levels, north Norfolk, England. *The Holocene*, *15*(2), 216-228.

Hurst, M. D., Rood, D. H., Ellis, M. A., Anderson, R. S., Dornbusch, U., 2016. Recent acceleration in coastal cliff retreat rates on the south coast of Great Britain. *Proceedings of the National Academy of Sciences*, *113* (47), 13336-13341.

Hurst, M. D., Rood, D. H., Ellis, M. A., 2017. Controls on the distribution of cosmogenic 10Be across shore platforms. *Earth Surface Dynamics*, *5*(1), 67-84.

Johnson, D. W., 1919. *Shore processes and shoreline development*. John Wiley & Sons, Incorporated.

Juignet P., 1974. La transgression crétacée sur la bordure orientale du Massif Armoricain. Thèse d'état, Université de Caen, 2 vol., 786p.

Kennedy, D. M., & Dickson, M. E., 2006. Lithological control on the elevation of shore platforms in a microtidal setting. *Earth Surface Processes and Landforms: The Journal of the British Geomorphological Research Group*, *31*(12), 1575-1584.

Lageat, Y., Hénaff, A., Costa, S., 2006. The retreat of the chalk cliffs of the Pays de Caux (France): erosion processes and patterns. *Annales de Géomorphologie/Annals of Geomorphology/Zeitschrift für Geomorphologie*, (144), 183-197.

Lal, D., 1991. Cosmic ray labeling of erosion surfaces: in situ nuclide production rates and erosion models. *Earth and Planetary Science Letters*, *104*(2-4), 424-439.

Lambeck, K., 1997. Sea-level change along the French Atlantic and Channel coasts since the time of the Last Glacial Maximum. *Palaeogeography, Palaeoclimatology, Palaeoecology*, *129* (1-2), 1-22.

Larsonneur, C., Vaslet, D., Auffret, J. P., 1979. Les sédiments superficiels de la Manche, Carte géologique de la marge continentale française. *Bureau des Recherches Géologiques et Minières, BRGM, Orléans*.

Lasseur E., 2007. La craie du Bassin de Paris (Cénomanien-Campanien, Crétacé Supérieur). Sédimentologie de faciès, stratigraphie séquentielle et géométrie 3D, *Thèse de Doctorat de l'Université de Rennes 1*, France, 423p.

Lasseur, E., Guillocheau, F., Robin, C., Hanot, F., Vaslet, D., Coueffe, R., Neraudeau, D., 2009. A relative water-depth model for the Normandy Chalk (Cenomanian–Middle Coniacian, Paris Basin, France) based on facies patterns of metre-scale cycles. *Sedimentary Geology*, *213* (1-2), 1-26.

Letortu, P., Costa, S., Bensaid, A., Cador, J. M., Quénol, H., 2014. Vitesses et modalités de recul des falaises crayeuses de Haute-Normandie (France): méthodologie et variabilité du recul. *Géomorphologie: relief, processus, environnement*, *20* (2), 133-144.

Letortu, P., Costa, S., Maquaire, O., Delacourt, C., Augereau, E., Davidson, R., Suanez, S., Nabucet, J., 2015. Retreat rates, modalities and agents responsible for erosion along the coastal chalk cliffs of Upper Normandy: The contribution of terrestrial laser scanning. *Geomorphology*, *245*, 3-14.

Letortu, P., Costa, S., Maquaire, O., Davidson, R., 2019. Marine and subaerial controls of coastal chalk cliff erosion in Normandy (France) based on a 7-year laser scanner monitoring. *Geomorphology*, 335, 76-91.

Lim, M., Rosser, N. J., Petley, D. N., Keen, M., 2011. Quantifying the controls and influence of tide and wave impacts on coastal rock cliff erosion. *Journal of Coastal Research*, *27*(1), 46-56.

Maillet, G., 2014. SPLASHALIOT-2 cruise, RV Haliotis, http://dx.doi.org/10.17600/14011800

Massey, A. C., Gehrels, W. R., Charman, D. J., Milne, G. A., Peltier, W. R., Lambeck, K., & Selby, K. A., 2008. Relative sea-level change and postglacial isostatic adjustment along the coast of south Devon, United Kingdom. *Journal of Quaternary Science: Published for the Quaternary Research Association*, *23*(5), 415-433.

Matsumoto H., Dickson M.E., Kench P.S., 2016, An exploratory numerical model of rocky shore profile evolution, *Geomorphology,* 268, 98-109.

Matsuoka, N., & Murton, J., 2008. Frost weathering: recent advances and future directions. *Permafrost and Periglacial Processes*, *19*(2), 195-210.

Mortimore R.N., 1997, The Chalk of Sussex and Kent, Geologist's Association Guide, N°57, The Geologist's Association, 1997.

Mortimore, R. N., 2001. Report on mapping of the chalk channel coast of France from Port du Havre-Antifer to Ault, June-September 2001. *Unpublished report, Brighton University*.

Mortimore, R., 2011. A chalk revolution: what have we done to the Chalk of England? *Proceedings of the Geologists' Association*, *122* (2), 232-297.

Mortimore, R. N., & Pomerol, B., 1987. Correlation of the upper cretaceous white chalk (Turonian to Campanian) in the Anglo-Paris Basin. *Proceedings of the Geologists' Association*, *98* (2), 97-143.

Mortimore, R. N., & Pomerol, B., 1991. Upper Cretaceous tectonic disruptions in a placid Chalk sequence in the Anglo-Paris Basin. *Journal of the Geological Society*, *148* (2), 391-404.

Mortimore, R., & Pomerol, B., 1997. Upper Cretaceous tectonic phases and end Cretaceous inversion in the Chalk of the Anglo-Paris Basin. *Proceedings of the geologists' association*, *108* (3), 231-255.

Mortimore, R. N., Wood, C. J., Gallois, R. W., 2001. *British upper Cretaceous stratigraphy* (Vol. 23). Joint Nature Conservation Committee (JNCC).

Mortimore, R. N., & Duperret, A. (Eds.)., 2004. Coastal chalk cliff instability. Geological Society of London.

Moses, C. A., Robinson, D. A., Williams, R. B. G., Marques, F. M. S. F., 2006. Predicting rates of shore platform downwearing from rock geotechnical properties and laboratory simulation of weathering and erosion processes. *Zeitschrift fur Geomorphologie Supplementband*, *144*, 19.

Naylor, L. A., & Stephenson, W. J., 2010. On the role of discontinuities in mediating shore platform erosion. *Geomorphology*, *114*(1-2), 89-100.

Neau, G., 1979. Carte géologique à 1/250 000 ème. Feuille de Rouen, BRGM, Orléans.

Parfitt S.A., Owen F., Keen D.H., 1998, Pleistocene stratigraphy, vertebrate and mullusca, Black Rock, Brighton. *in* : Murton J.B., Whiteman C.A., Bates M.R., Bridgland D.R., Long A.J., Roberts M.B. and Walker M.P. (eds). Tha Quaternary of Kent and Sussex : Field Guide, Quaternary Research Association, London, 146-150.

Peregrine, D. H., Kalliadasis, S., 1996. Filling flows, cliff erosion and cleaning flows. *Journal of Fluid Mechanics*, *310*, 365-374.

Prémaillon, M., Regard, V., Dewez, T. J., Auda, Y., 2018. GlobR2C2 (Global Recession Rates of Coastal Cliffs): a global relational database to investigate coastal rocky cliff erosion rate variations. *Earth Surface Dynamics*, *6*(3).

Raimbault, C., Duperret, A., Regard, V., Molliex, S., Wyns, R., Authemayou, C., Le Gall, B., 2018a. Quaternary geomorphological evolution of a granitic shore platform constrained by in situ 10Be concentrations, Penmarc'h, SW Brittany, France. *Marine Geology*, *395*, 33-47.

Raimbault, C., Duperret, A., Le Gall, B., Authemayou, C., 2018b. Structural inheritance and coastal geomorphology in SW Brittany, France: An onshore/offshore integrated approach. *Geomorphology*, *306*, 141-154.

Regard, V., Dewez, T., Bourles, D. L., Anderson, R. S., Duperret, A., Costa, S., Maillet, G. M., 2012. Late Holocene seacliff retreat recorded by 10Be profiles across a coastal platform: Theory and example from the English Channel. *Quaternary Geochronology*, *11*, 87-97.

Regard, V., Dewez, T. J., Cnudde, C., Hourizadeh, N., 2013. Coastal chalk platform erosion modulated by step erosion and debris shielding: example from Normandy and Picardy (northern France). *Journal of Coastal Research*, *65*(sp2), 1692-1698.

Rodet, J., 1983. Karst et littoral du Bec de Caux (Seine-Maritime, Normandie, France). *Karstologia*, *2*(1), 23-32.

Senfaute, G., Duperret, A., Lawrence, J. A., 2009. Micro-seismic precursory cracks prior to rock-fall on coastal chalk cliffs: a case study at Mesnil-Val, Normandie, NW France. *Natural Hazards and Earth System Sciences*, *9* (5), 1625-1641.

Shennan, I., Milne, G., & Bradley, S., 2012. Late Holocene vertical land motion and relative sea-level changes: lessons from the British Isles. *Journal of Quaternary Science*, *27*(1), 64-70.

SHOM, 2017. Références Altimétriques Marines. Ports de France métropolitaine et d'outre-mer. Côtes du zéro hydrographique et niveaux caractéristiques de la marée. https://diffusion.shom.fr/pro/references-altimetriques-maritimes-ram.html

Stephenson, W. J., & Kirk, R. M., 2000. Development of shore platforms on Kaikoura Peninsula, South Island, New Zealand: Part one: the role of waves. *Geomorphology*, *32*(1-2), 21-41.

Siddall, M., Chappell, J., Potter, E. K., 2007. 7. Eustatic sea level during past interglacials. In *Developments in Quaternary Sciences* (Vol. 7, pp. 75-92). Elsevier.

Smith B., 1936, Levels in the raised beach, Black Rock, Brighton. Geological Magazine, 73, 423-426.

Sommé J., Antoine P., Cunat-Boge N., Lefevre D., Munaut A.V., 1999, Le Pleistocene moyen de la mer du Nord en France. Falaise de Sangatte et formation de Herzeele, Quaternaire, 10, 151-160.

Sunamura, T., 1977. A relationship between wave-induced cliff erosion and erosive force of waves. *The Journal of Geology*, *85*(5), 613-618.

Sunamura, T., 1983. Processes of sea cliff and platform erosion. *CRC handbook of coastal processes and erosion*, 233-265.

Sunamura, T., 1992. *Geomorphology of rocky coasts* (Vol. 302). Chichester: Wiley.

Swirad Z.M, 2018, Multi-scale assessment of shore platform erosion, Doctoral PhD thesis, Durham University, UK.

Swirad Z.M., Rosser N.J., Brain M.J., Rood D.H., Hurst M.D., Wilcken K.M, Barlow J., 2020, Cosmogenic exposure dating reveals limited long-term variability in erosion of a rocky coastline, *Nature Communications*, (2020) 11:3804

Tessier, B., Billeaud, I., Sorrel, P., Delsinne, N., Lesueur, P., 2012. Infilling stratigraphy of macrotidal tide-dominated estuaries. Controlling mechanisms: Sea-level fluctuations, bedrock morphology, sediment supply and climate changes (The examples of the Seine estuary and the Mont-Saint-Michel Bay, English Channel, NW France). *Sedimentary Geology*, *279*, 62-73.

Trenhaile, A. S., 1978. The shore platforms of Gaspé, Québec. *Annals of the Association of American Geographers*, *68*(1), 95-114.

Trenhaile, A. S., 1980. Shore platforms: a neglected coastal feature. *Progress in physical geography*, *4*(1), 1-23.

Trenhaile, A. S., 1987. *The geomorphology of rock coasts*. Oxford University Press, USA.

Trenhaile, A. S., 1999. The width of shore platforms in Britain, Canada, and Japan. *Journal of Coastal Research*, 355-364.

Trenhaile, A. S., 2000. Modeling the development of wave-cut shore platforms. *Marine Geology*, *166* (1-4), 163-178.

Trenhaile, A. S., 2001a. Modelling the Quaternary evolution of shore platforms and erosional continental shelves. *Earth Surface Processes and Landforms: The Journal of the British Geomorphological Research Group*, *26* (10), 1103-1128.

Trenhaile, A. S., 2001b. Modeling the effect of late Quaternary interglacial sea levels on wave-cut shore platforms. *Marine Geology*, *172* (3-4), 205-223.

Trenhaile, A. S., 2002. Rock coasts, with particular emphasis on shore platforms. *Geomorphology*, *48*(1-3), 7-22.

Walkden, M. J. A., & Hall, J. W., 2005. A predictive mesoscale model of the erosion and profile development of soft rock shores. *Coastal Engineering*, *52*(6), 535-563.

Wright, L. W. 1970. Variation in the level of the cliff/shore platform junction along the south coast of Great Britain. *Marine Geology*, *9* (5), 347-353.

Young, A. P., Adams, P. N., O'Reilly, W. C., Flick, R. E., Guza, R. T., 2011. Coastal cliff ground motions from local ocean swell and infragravity waves in southern California. *Journal of Geophysical Research: Oceans*, *116*(C9).

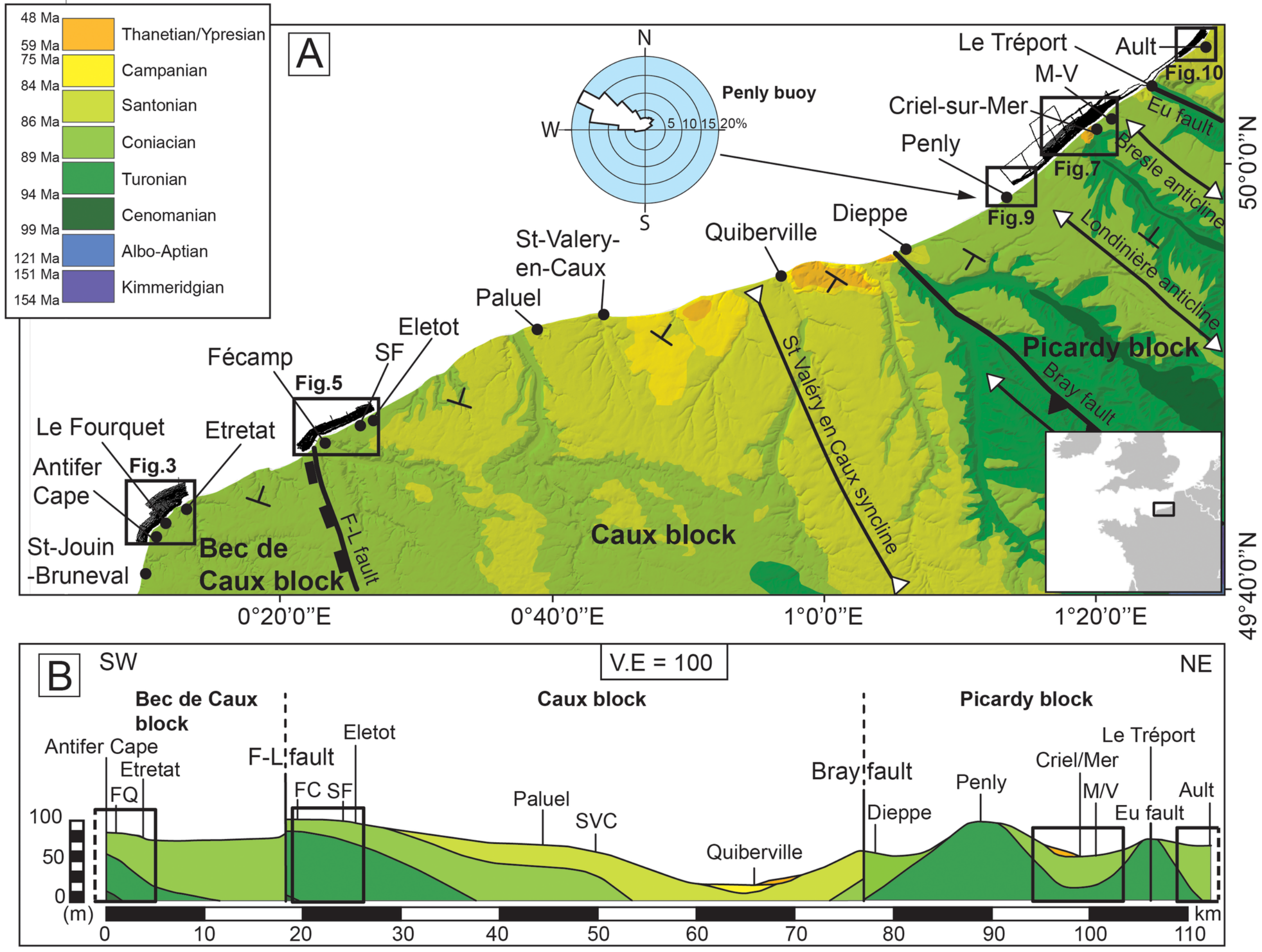

48 Ma
59 Ma
Thanetian/Ypresian
75 Ma
84 Ma
Campanian
Santonian
86 Ma
Coniacian
89 Ma
Turonian
94 Ma
Cenomanian
99 Ma
Albo-Aptian
121 Ma
151 Ma
Kimmeridgian
154 Ma
A
N
S
W
Penly buoy
5 10 15 20%
Le Tréport
Ault
Fig.10
M-V
Criel-sur-Mer
Eu fault
Fig.7
Penly
Bresle anticline
Fig.9
Dieppe
Londinière anticline
Quiberville
St-Valery-en-Caux
Paluel
Picardy block
Bray fault
Eletot
SF
Fécamp
Fig.5
St Valéry en Caux syncline
Le Fourquet
Etretat
Antifer Cape
Fig.3
St-Jouin-Bruneval
Bec de Caux block
F-L fault
Caux block
50°0'0"N
49°40'0"N
0°20'0"E
0°40'0"E
1°0'0"E
1°20'0"E
B
SW
V.E = 100
NE
Bec de Caux block
Caux block
Picardy block
Antifer Cape
Etretat
FQ
F-L fault
Eletot
FC SF
Paluel
SVC
Quiberville
Bray fault
Dieppe
Penly
Criel/Mer
M/V
Le Tréport
Eu fault
Ault
100
50
0
(m)
0 10 20 30 40 50 60 70 80 90 100 110
km

| System | Stage | Formations in Sussex | Key markers | Additional features in Normandy | Formations in Normandy | Local Formations used in Normandy (Lasseur, 2007) | | Local Formations used in Hauts de France (Amedro and Robaszynski, 2000) |
|---|---|---|---|---|---|---|---|---|
| Upper Cretaceous | **Campanian** | **Culver Chalk** | *Castle Hill marl* | *no outcrops* | | | | |
| | | **Newhaven Chalk** | *Telscoombe marls* | | | | | |
| | | | *Meeching marls* | | | | | |
| | | | *Peacehaven marl* | | | | | |
| | | | *Old Nore marl* | | **Newhaven Chalk** | craie de Vasterival | | Caffiers |
| | **Santonian** | | *Friar's bay marl* | | | | | |
| | | | *Brighton marl* | Quiberville HG | | craie de Sotteville | | |
| | | | *Buckle marl* | | | | | |
| | | **Seaford Chalk** | *Exceat flint* | | **Seaford Chalk** | craie de Veulettes | | |
| | | | *Whitaker's three inch flint* | | | | | |
| | | | *Bedwell's columnar flint* | | | | | |
| | **Coniacian** | | *Seven Sisters flint band* | St valery HGs | | | | |
| | | | *Belle Tout marls* | Etretat Complex | | | | |
| | | | *Shoreham marls* | | | | | |
| | | **Lewes Nodular Chalk** | *Light Point HGs* | | **Lewes Nodular Chalk** | craie de Saint Pierre en Port | craie de Petites Dalles | |
| | | | *Beeding HGs* | | | | | |
| | | | *Hope Gap HGs* | | | | | |
| | | | *Cliffe HG* | | | | | |
| | | | *Navigation marl* | | | | craie d' Eletot | |
| | **Turonian** | | *Lewes marl* | | | | | |
| | | | *Bridgewick marl* | | | | | Guet |
| | | | *Cabum marl* | Mers HGs | | craie de Senneville | | |
| | | | *Southerham marl* | | | | | |
| | | | *Glynde marl* | | | | | |
| | | **New Pit Chalk** | *New Pit marls* | 3 Tilleul HGs | **New Pit Chalk** | craie du Val st Nicolas | | Mottelettes |
| | | | *Malling street marl* | | | | | |
| | | | *Glyndebourne flints* | | | | | |
| | | | *Gun Gardens main marl* | | | | | |
| | | **Holywell Nodular Chalk** | *Meads marls* | | **Holywell Nodular Chalk** | craie du Cap Fagnet | | Grand Blanc-Nez |
| | **Cenomanian** | | *Plenus marl* | Antifer HGs | | craie d'Antifer | | Crupes |
| | | **Zig Zag Chalk** | *Tenuis limestone* | | **Craie de Rouen** | craie de Rouen | | Escalles |
| | | | | | | | | Cran |
| | | **West Melbury Marly Chalk** | *Glauconitic marl* | | **Glauconitic Chalk** | craie glauconieuse | | Petit Blanc-Nez |
| | | | | | | | | Strouanne |

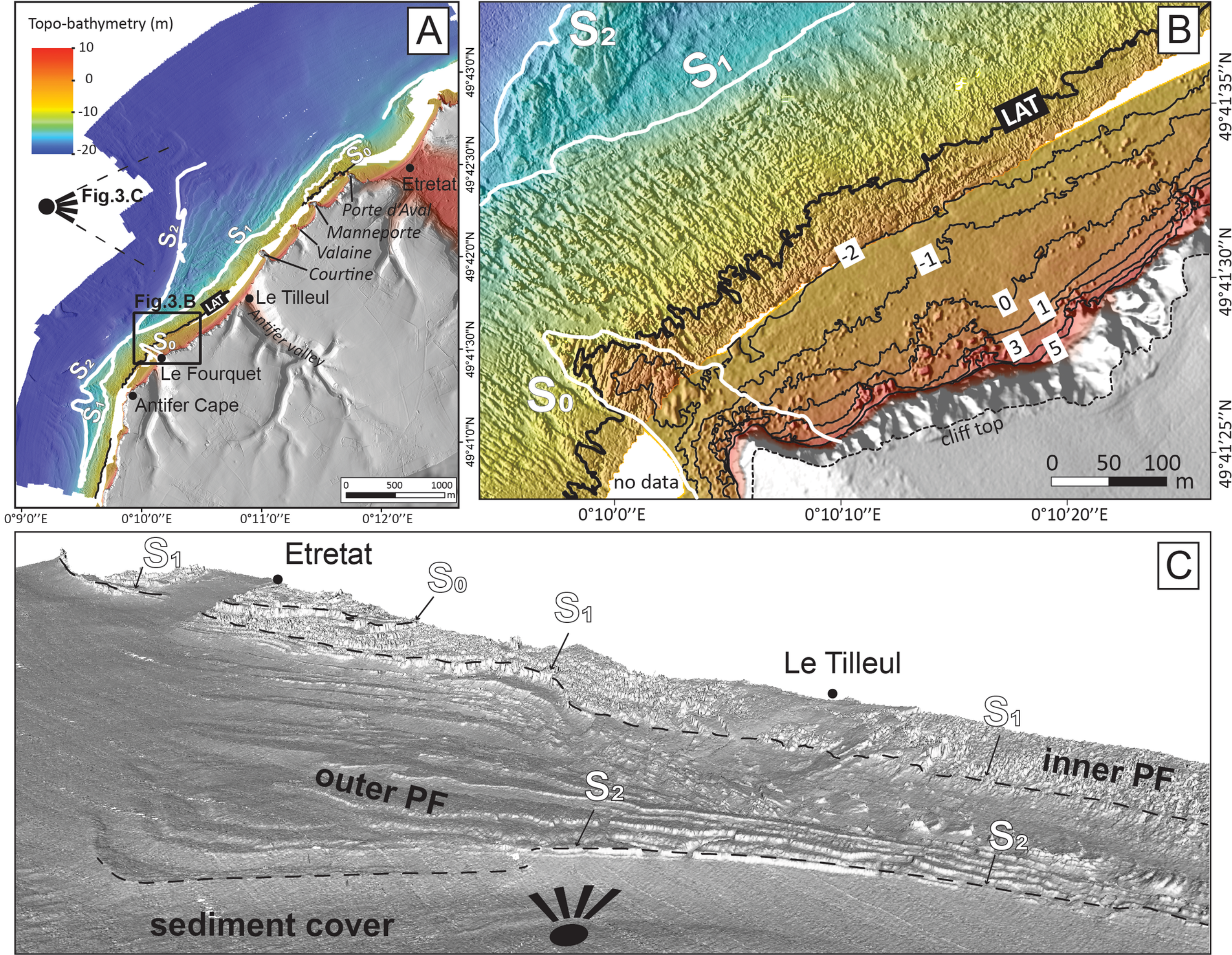
A
Topo-bathymetry (m)
10
0
-10
-20
Fig.3.C
S2
S1
S0
LAT
Etretat
Porte d'Aval
Manneporte
Valaine
Courtine
Le Tilleul
Antifer valley
Fig.3.B
Le Fourquet
Antifer Cape
0 500 1000 m
49°43'0''N
49°42'30''N
49°42'0''N
49°41'30''N
49°41'0''N
0°9'0''E
0°10'0''E
0°11'0''E
0°12'0''E
B
S2
S1
S0
LAT
-2
-1
0
1
3
5
cliff top
no data
0 50 100 m
49°41'35''N
49°41'30''N
49°41'25''N
0°10'0''E
0°10'10''E
0°10'20''E
C
S1
Etretat
S0
S1
Le Tilleul
S1
inner PF
outer PF
S2
S2
sediment cover

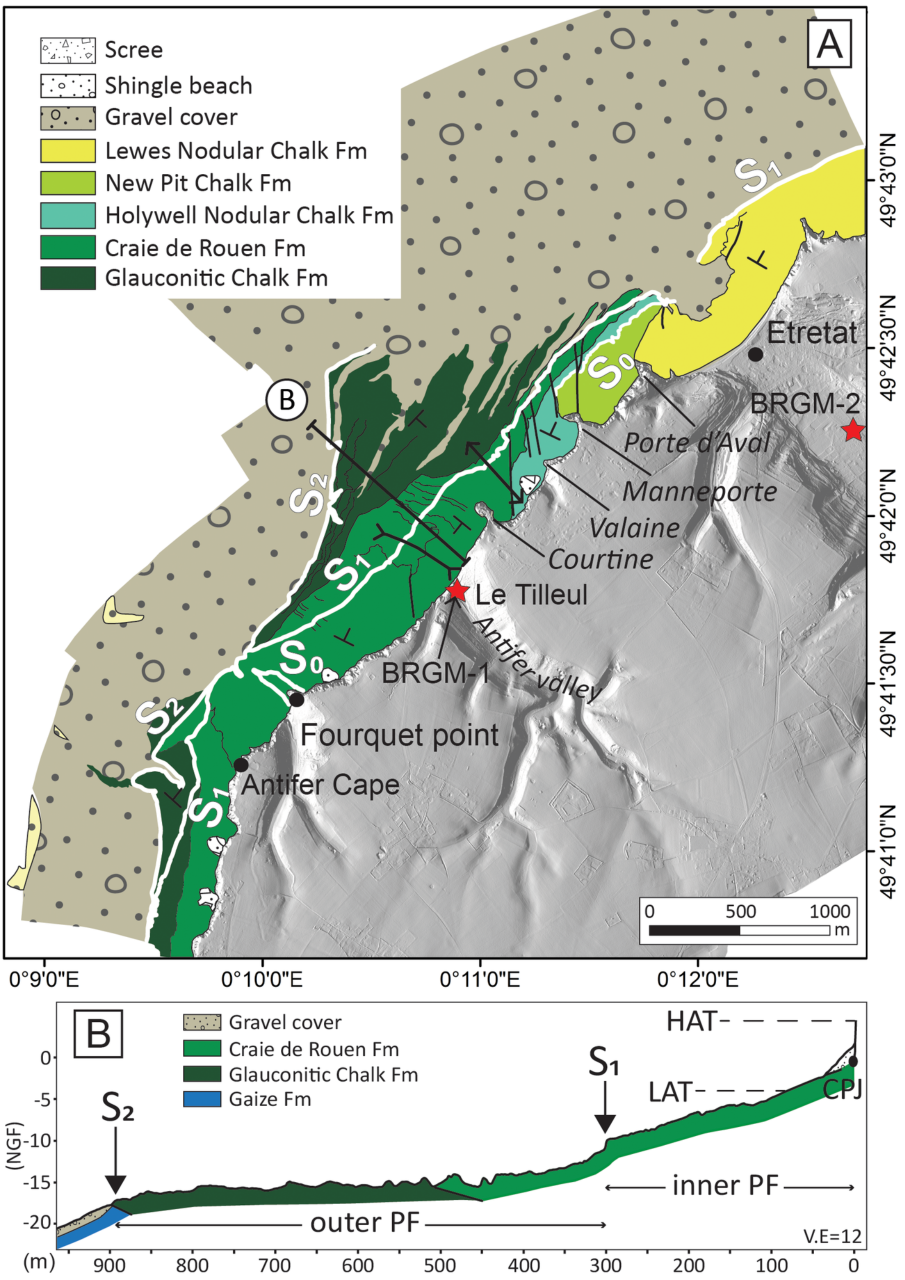

A
Scree
Shingle beach
Gravel cover
Lewes Nodular Chalk Fm
New Pit Chalk Fm
Holywell Nodular Chalk Fm
Craie de Rouen Fm
Glauconitic Chalk Fm
S1
S0
S2
Etretat
BRGM-2
Porte d'Aval
Manneporte
Valaine
Courtine
Le Tilleul
Antifer valley
BRGM-1
Fourquet point
Antifer Cape
0 500 1000 m
49°43'0"N
49°42'30"N
49°42'0"N
49°41'30"N
49°41'0"N
0°9'0"E
0°10'0"E
0°11'0"E
0°12'0"E
B
Gravel cover
Craie de Rouen Fm
Glauconitic Chalk Fm
Gaize Fm
HAT
LAT
CPJ
inner PF
outer PF
(NGF)
V.E=12
(m)

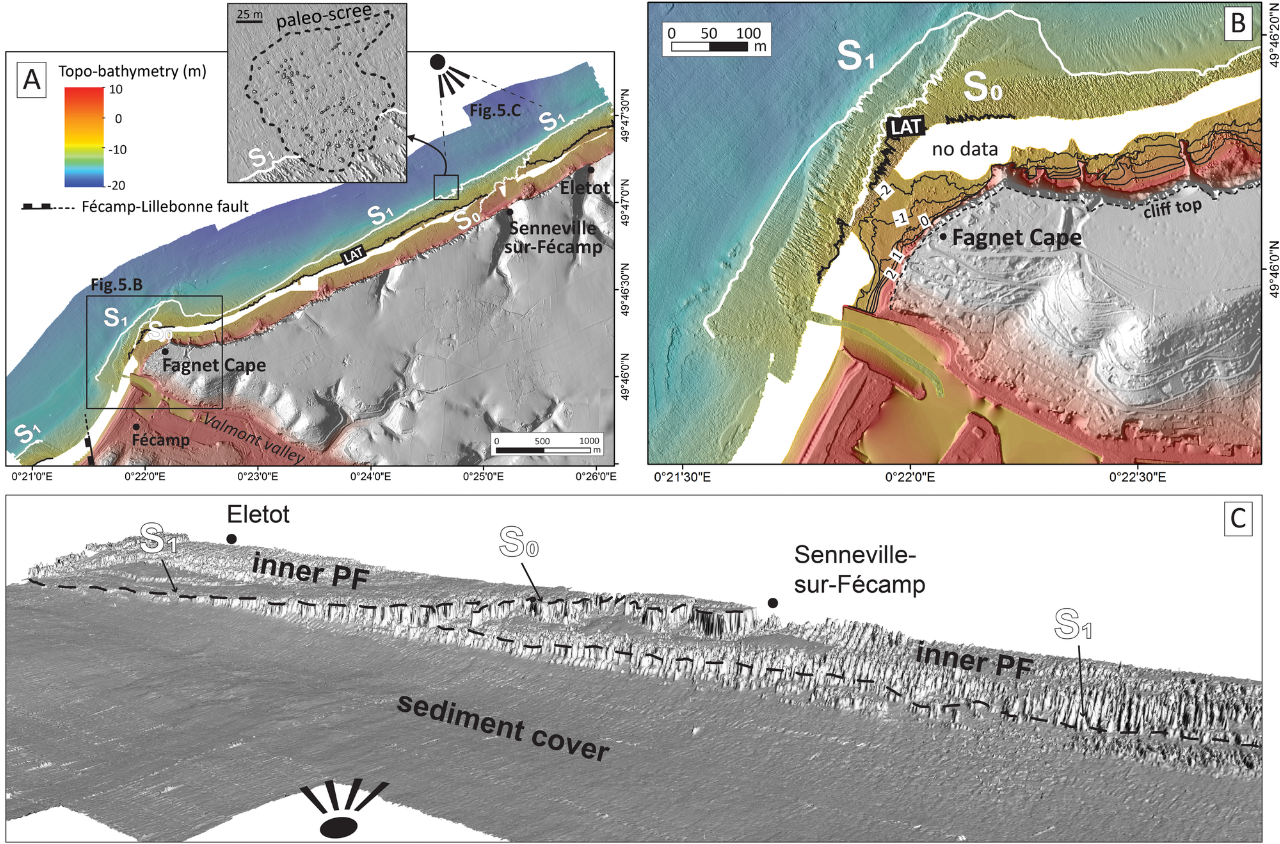
A
Topo-bathymetry (m)
10
0
-10
-20
Fécamp-Lillebonne fault
paleo-scree
25 m
Fig.5.C
Fig.5.B
S1
S0
LAT
Eletot
Senneville sur-Fécamp
Fagnet Cape
Fécamp
Valmont valley
0 500 1000 m
0°21'0"E
0°22'0"E
0°23'0"E
0°24'0"E
0°25'0"E
0°26'0"E
49°47'30"N
49°47'0"N
49°46'30"N
49°46'0"N
B
0 50 100 m
no data
cliff top
Fagnet Cape
-2
-1
0
1
2
0°21'30"E
0°22'0"E
0°22'30"E
49°46'20"N
49°46'0"N
C
Eletot
Senneville-sur-Fécamp
inner PF
sediment cover

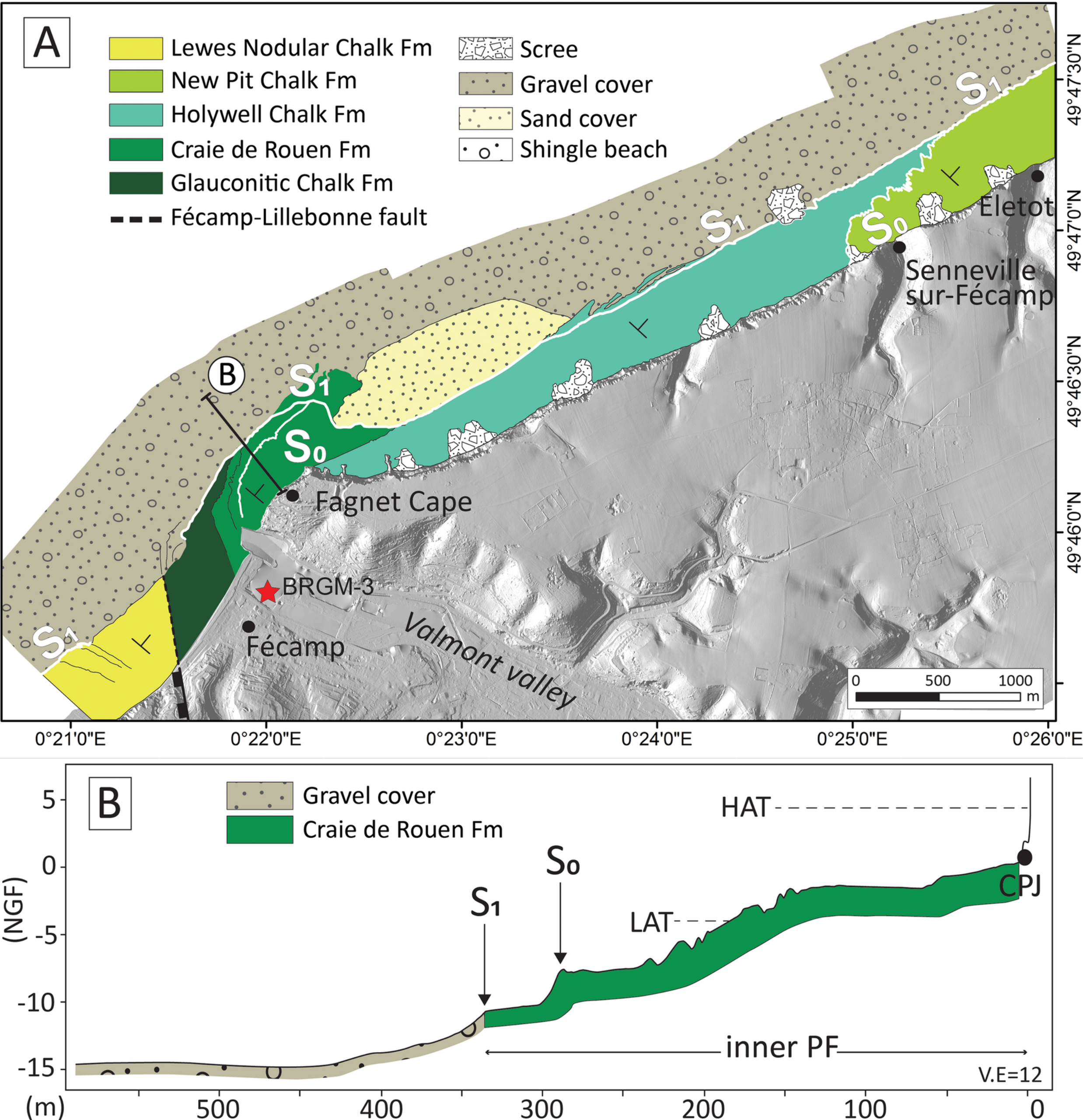
A
Lewes Nodular Chalk Fm
New Pit Chalk Fm
Holywell Chalk Fm
Craie de Rouen Fm
Glauconitic Chalk Fm
Fécamp-Lillebonne fault
Scree
Gravel cover
Sand cover
Shingle beach
S1
S0
Eletot
Senneville sur-Fécamp
Fagnet Cape
BRGM-3
Fécamp
Valmont valley
B
0 500 1000 m
49°47'30"N
49°47'0"N
49°46'30"N
49°46'0"N
0°21'0"E
0°22'0"E
0°23'0"E
0°24'0"E
0°25'0"E
0°26'0"E
B
Gravel cover
Craie de Rouen Fm
HAT
LAT
CPJ
S1
S0
inner PF
V.E=12
(NGF)
5
0
-5
-10
-15
(m)
500
400
300
200
100
0

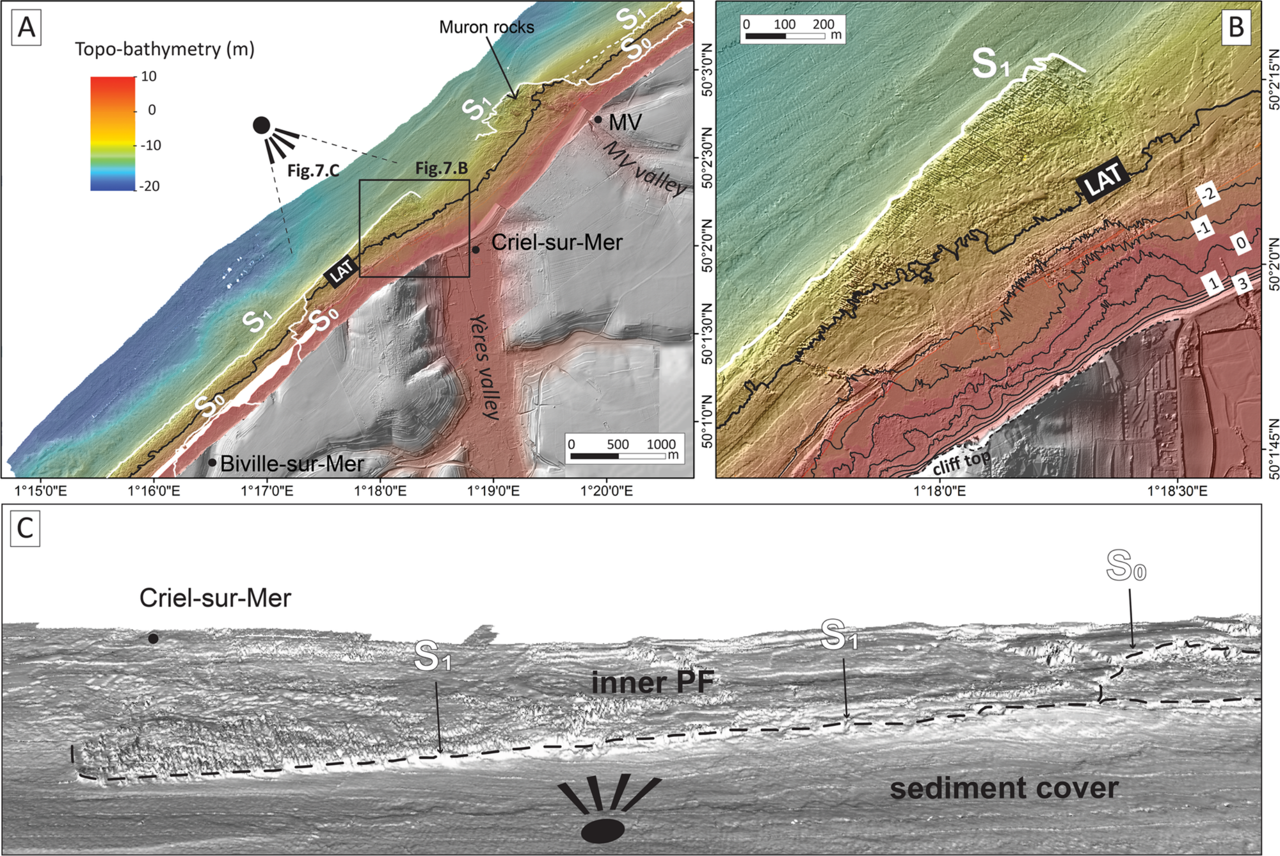

A
Topo-bathymetry (m)
10
0
-10
-20
Muron rocks
S1
S0
MV
MV valley
Fig.7.C
Fig.7.B
Criel-sur-Mer
LAT
Yères valley
Biville-sur-Mer
0 500 1000 m
50°3'0"N
50°2'30"N
50°2'0"N
50°1'30"N
50°1'0"N
1°15'0"E
1°16'0"E
1°17'0"E
1°18'0"E
1°19'0"E
1°20'0"E
B
0 100 200 m
-2
-1
0
1
3
cliff top
50°2'15"N
50°2'0"N
50°1'45"N
1°18'0"E
1°18'30"E
C
Criel-sur-Mer
inner PF
sediment cover

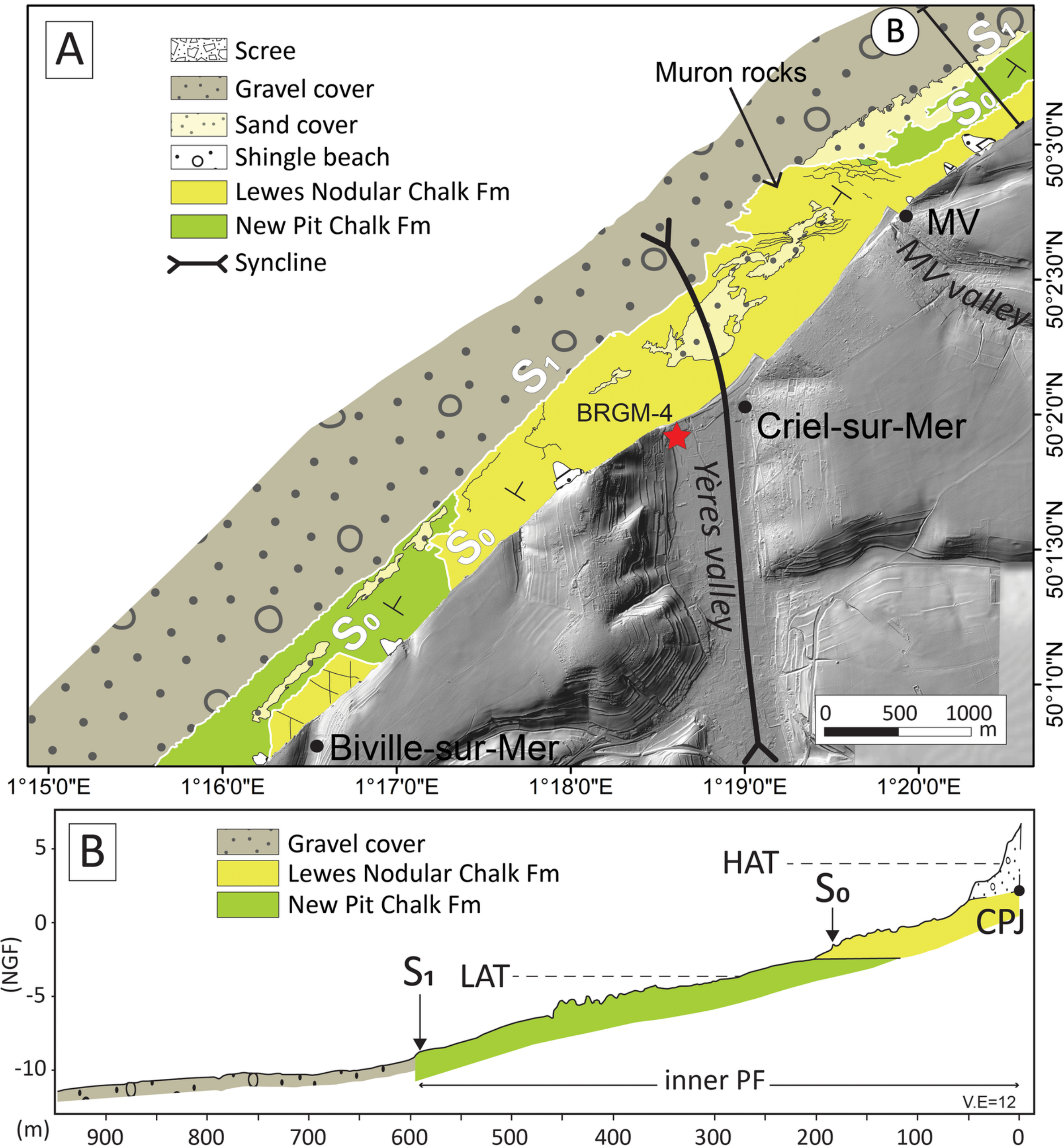

A
Scree
Gravel cover
Sand cover
Shingle beach
Lewes Nodular Chalk Fm
New Pit Chalk Fm
Syncline
B
Muron rocks
S1
S0
MV
MV valley
BRGM-4
Criel-sur-Mer
Yères valley
Biville-sur-Mer
0 500 1000 m
50°3'0"N
50°2'30"N
50°2'0"N
50°1'30"N
50°1'0"N
1°15'0"E
1°16'0"E
1°17'0"E
1°18'0"E
1°19'0"E
1°20'0"E
B
Gravel cover
Lewes Nodular Chalk Fm
New Pit Chalk Fm
HAT
S0
CPJ
S1
LAT
inner PF
V.E=12
(NGF)
(m)
5
0
-5
-10
900
800
700
600
500
400
300
200
100
0

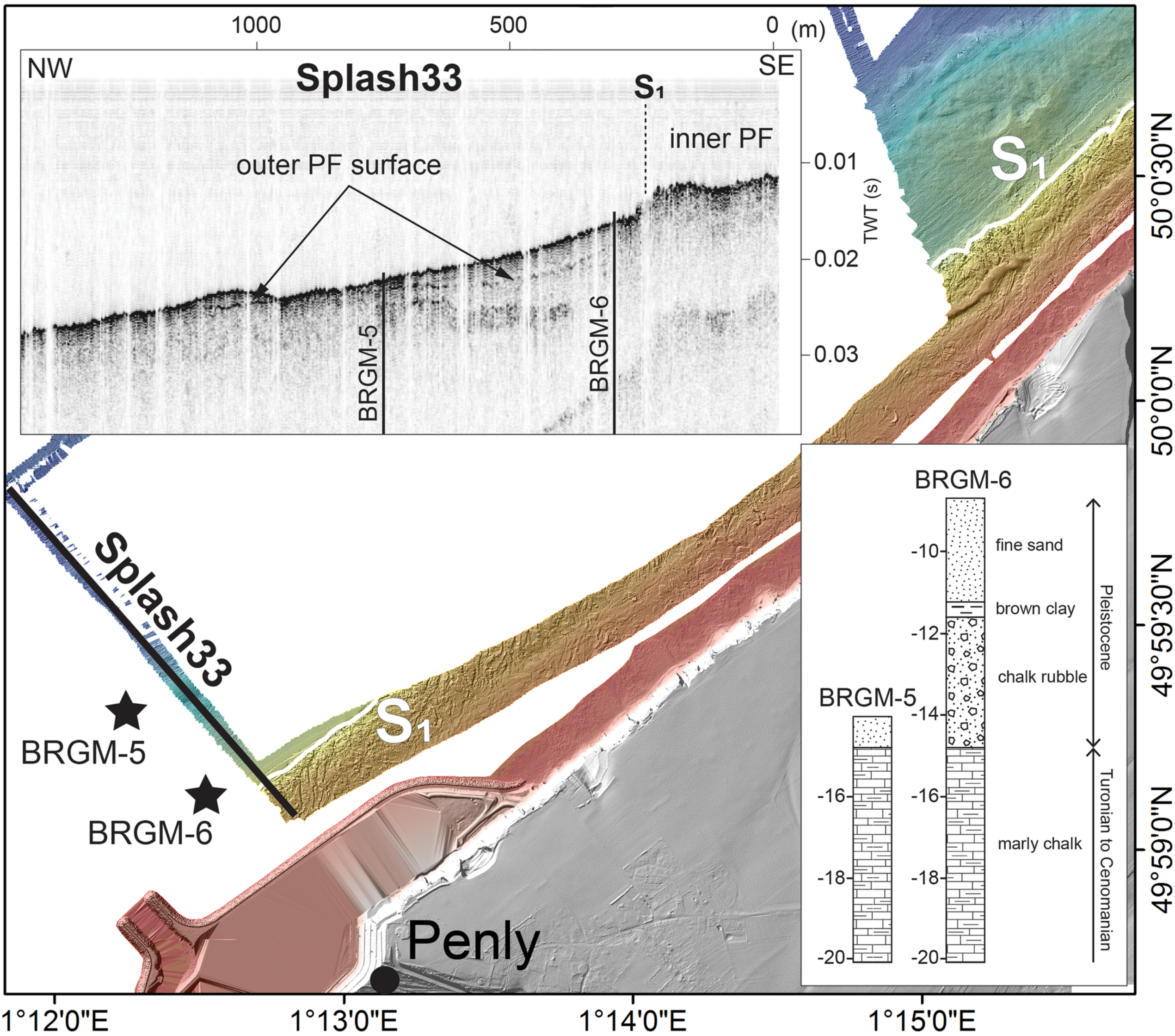

1000
500
0 (m)
NW
SE
Splash33
S1
inner PF
outer PF surface
TWT (s)
0.01
0.02
0.03
BRGM-5
BRGM-6
Splash33
S1
S1
BRGM-5
BRGM-6
Penly
BRGM-6
BRGM-5
fine sand
brown clay
chalk rubble
marly chalk
Pleistocene
Turonian to Cenomanian
-10
-12
-14
-16
-18
-20
50°0'30"N
50°0'0"N
49°59'30"N
49°59'0"N
1°12'0"E
1°13'0"E
1°14'0"E
1°15'0"E

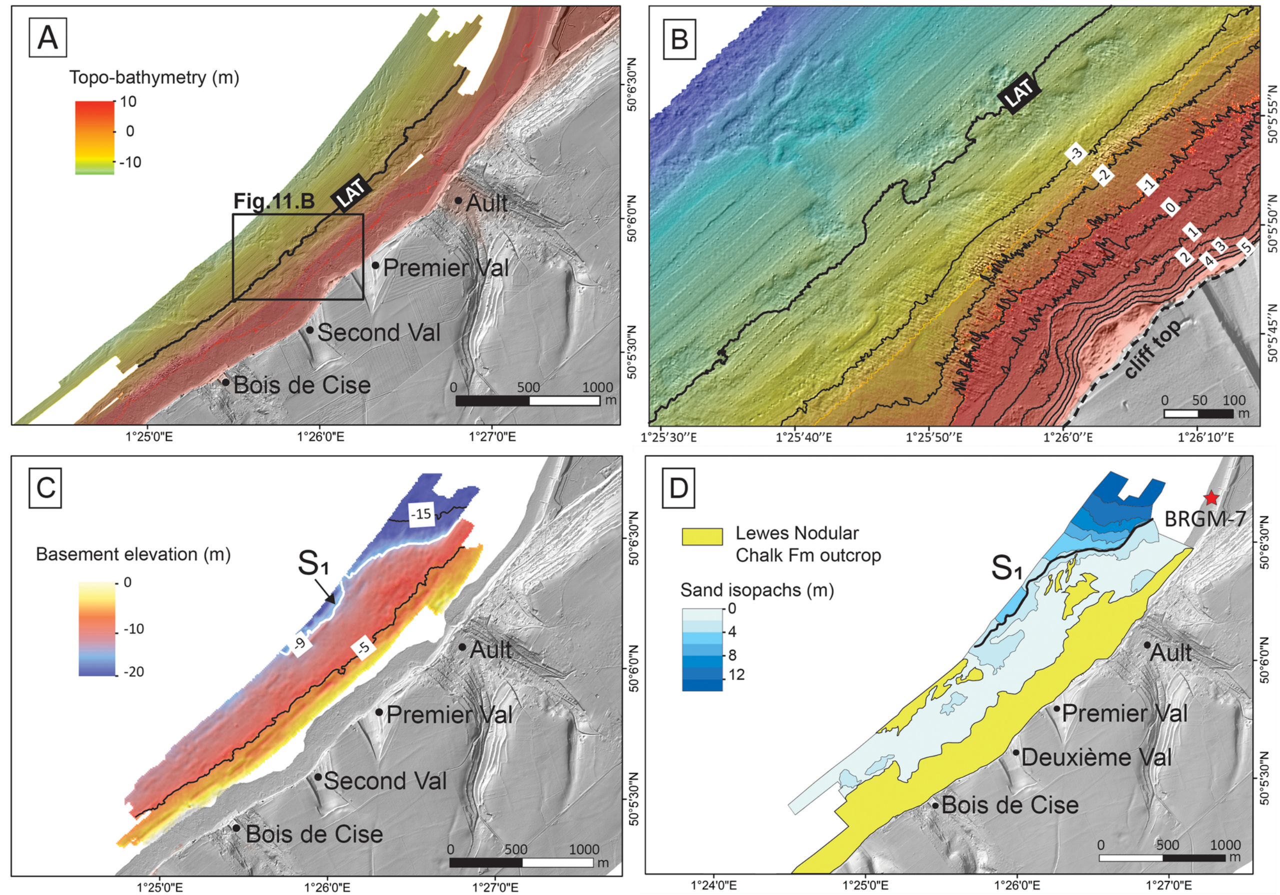

A
Topo-bathymetry (m)
10
0
-10
Fig.11.B
LAT
Ault
Premier Val
Second Val
Bois de Cise
0
500
1000
m
50°6'30"N
50°6'0"N
50°5'30"N
1°25'0"E
1°26'0"E
1°27'0"E
B
LAT
-3
-2
-1
0
1
2
3
4
5
cliff top
0
50
100
m
50°5'55"N
50°5'50"N
50°5'45"N
1°25'30"E
1°25'40"E
1°25'50"E
1°26'0"E
1°26'10"E
C
Basement elevation (m)
0
-10
-20
S1
-15
-9
-5
Ault
Premier Val
Second Val
Bois de Cise
0
500
1000
m
50°6'30"N
50°6'0"N
50°5'30"N
1°25'0"E
1°26'0"E
1°27'0"E
D
Lewes Nodular
Chalk Fm outcrop
Sand isopachs (m)
0
4
8
12
S1
BRGM-7
Ault
Premier Val
Deuxième Val
Bois de Cise
0
500
1000
m
50°6'30"N
50°6'0"N
50°5'30"N
1°24'0"E
1°25'0"E
1°26'0"E
1°27'0"E

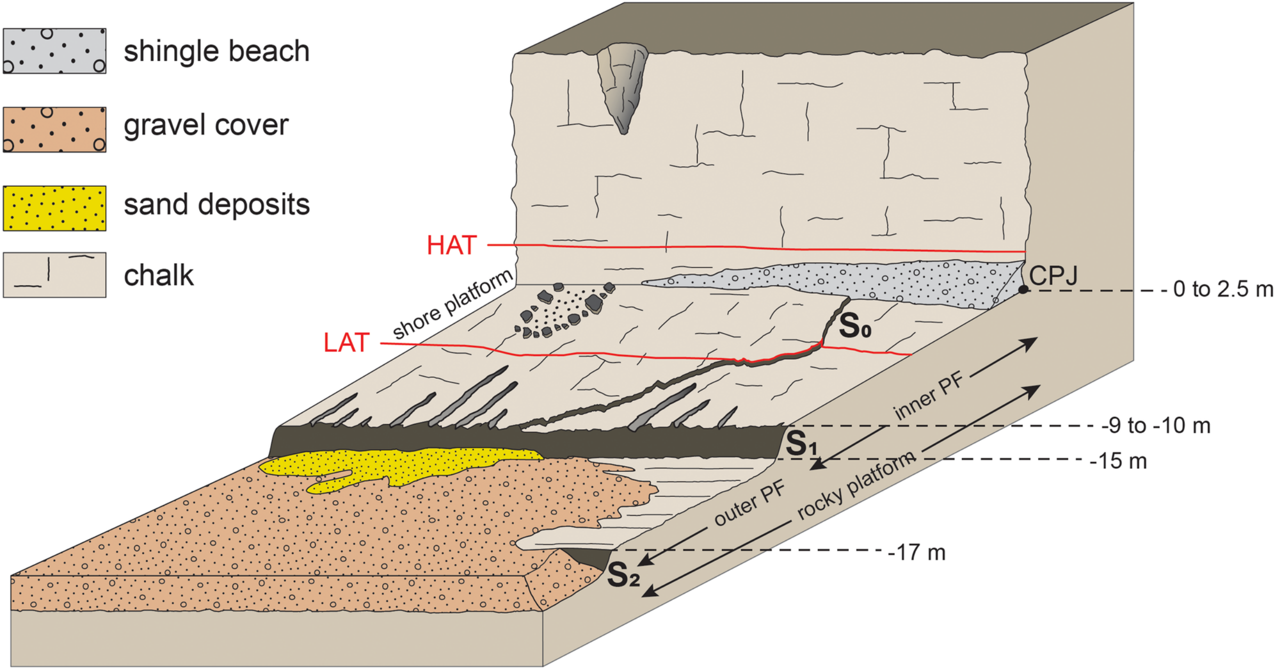
shingle beach
gravel cover
sand deposits
chalk
HAT
LAT
shore platform
CPJ
0 to 2.5 m
$S_0$
$S_1$
$S_2$
inner PF
outer PF
rocky platform
-9 to -10 m
-15 m
-17 m

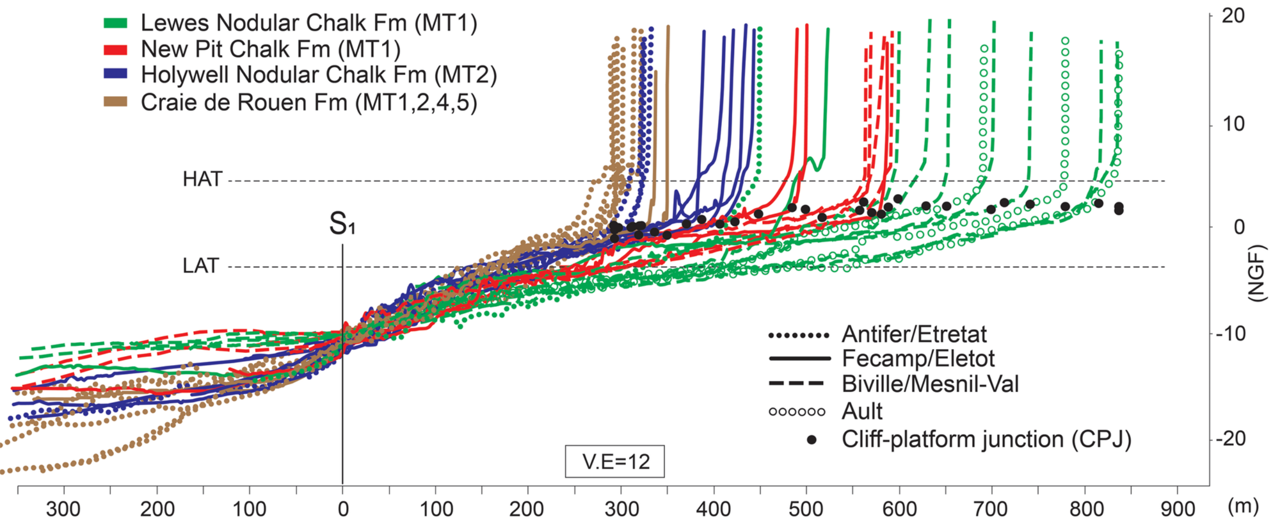

Lewes Nodular Chalk Fm (MT1)
New Pit Chalk Fm (MT1)
Holywell Nodular Chalk Fm (MT2)
Craie de Rouen Fm (MT1,2,4,5)
HAT
LAT
S1
Antifer/Etretat
Fecamp/Eletot
Biville/Mesnil-Val
Ault
Cliff-platform junction (CPJ)
V.E=12
20
10
0
-10
-20
(NGF)
300
200
100
0
100
200
300
400
500
600
700
800
900
(m)

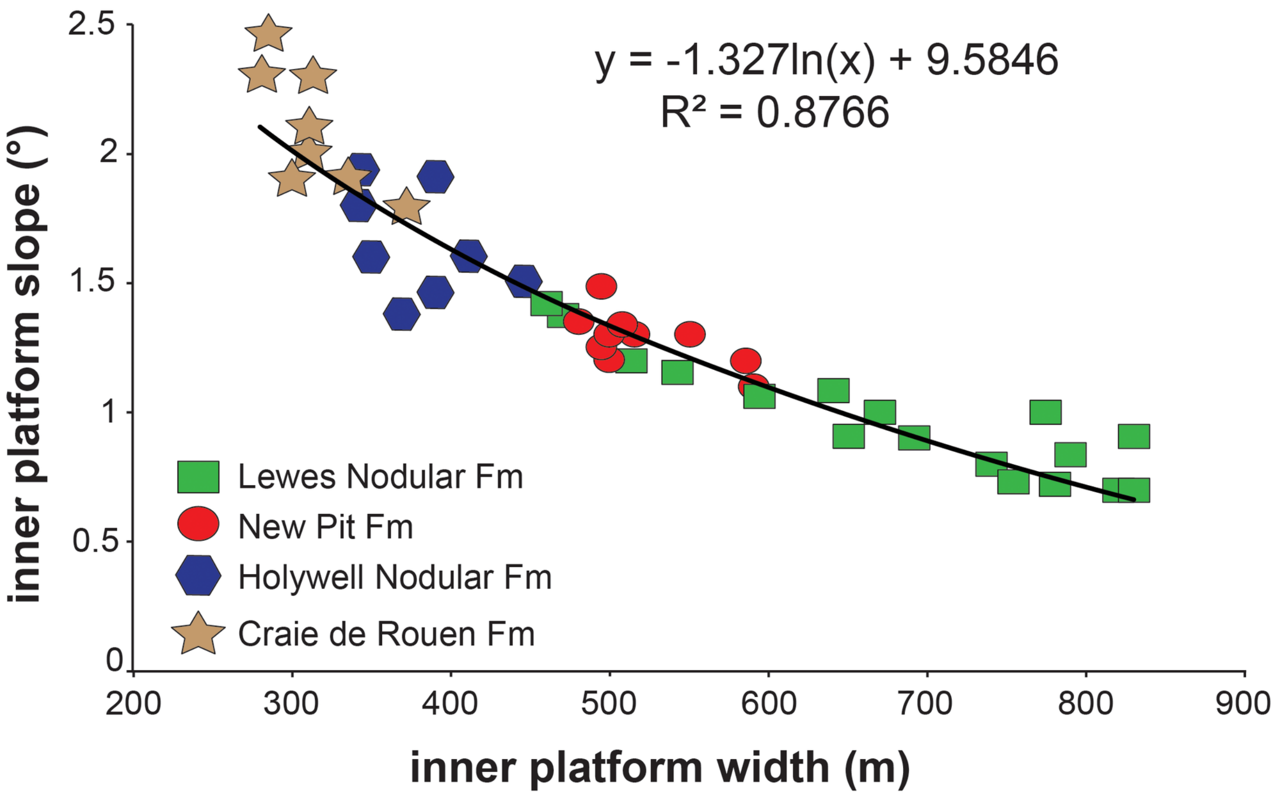
y = -1.327ln(x) + 9.5846
R² = 0.8766
inner platform slope (°)
inner platform width (m)
2.5
2
1.5
1
0.5
0
200
300
400
500
600
700
800
900
Lewes Nodular Fm
New Pit Fm
Holywell Nodular Fm
Craie de Rouen Fm

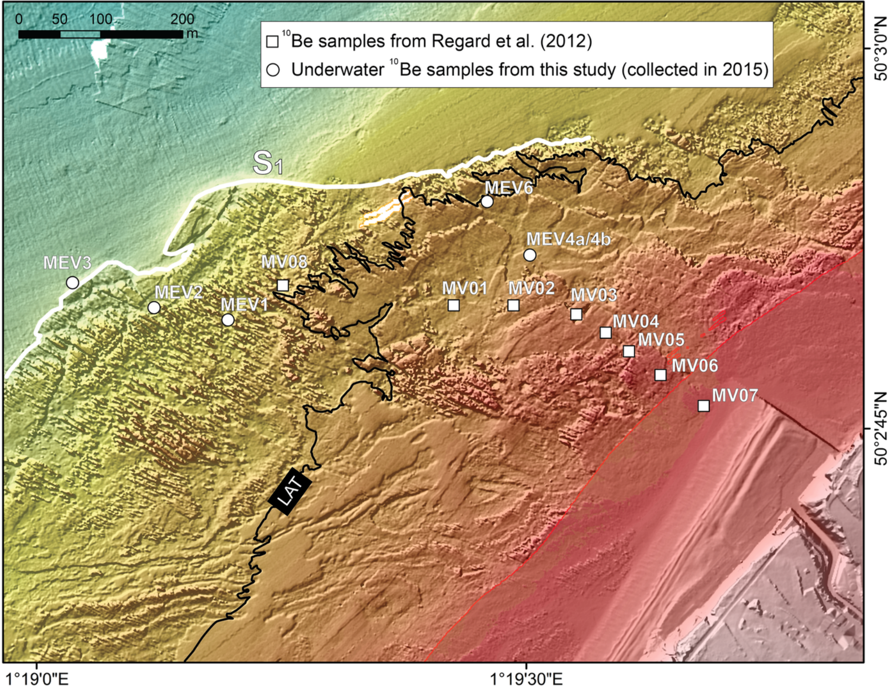
0 50 100 200 m
10Be samples from Regard et al. (2012)
Underwater 10Be samples from this study (collected in 2015)
S1
MEV6
MEV4a/4b
MEV3
MV08
MEV2
MEV1
MV01
MV02
MV03
MV04
MV05
MV06
MV07
LAT
50°3'0"N
50°2'45"N
1°19'0"E
1°19'30"E

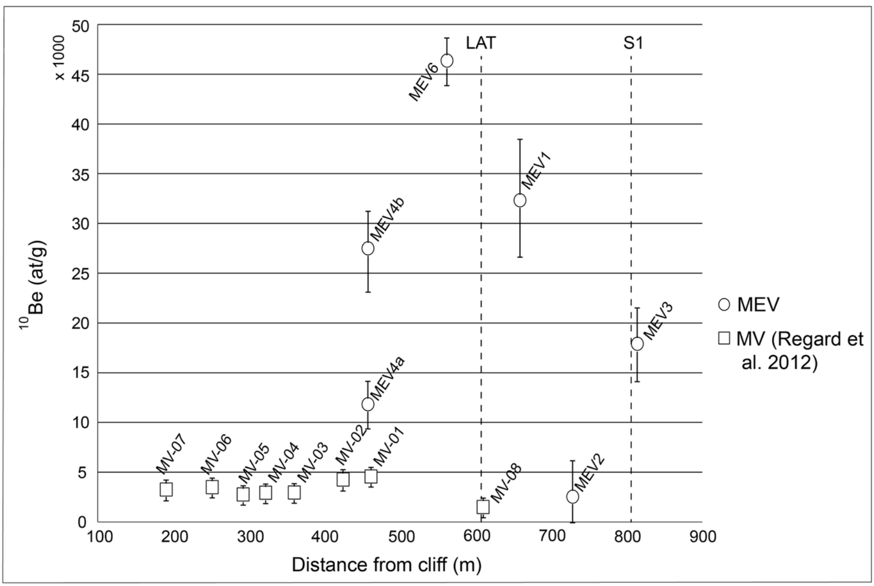
10Be (at/g)
x 1000
Distance from cliff (m)
LAT
S1
MEV6
MEV1
MEV4b
MEV3
MEV4a
MV-07
MV-06
MV-05
MV-04
MV-03
MV-02
MV-01
MV-08
MEV2
MEV
MV (Regard et al. 2012)

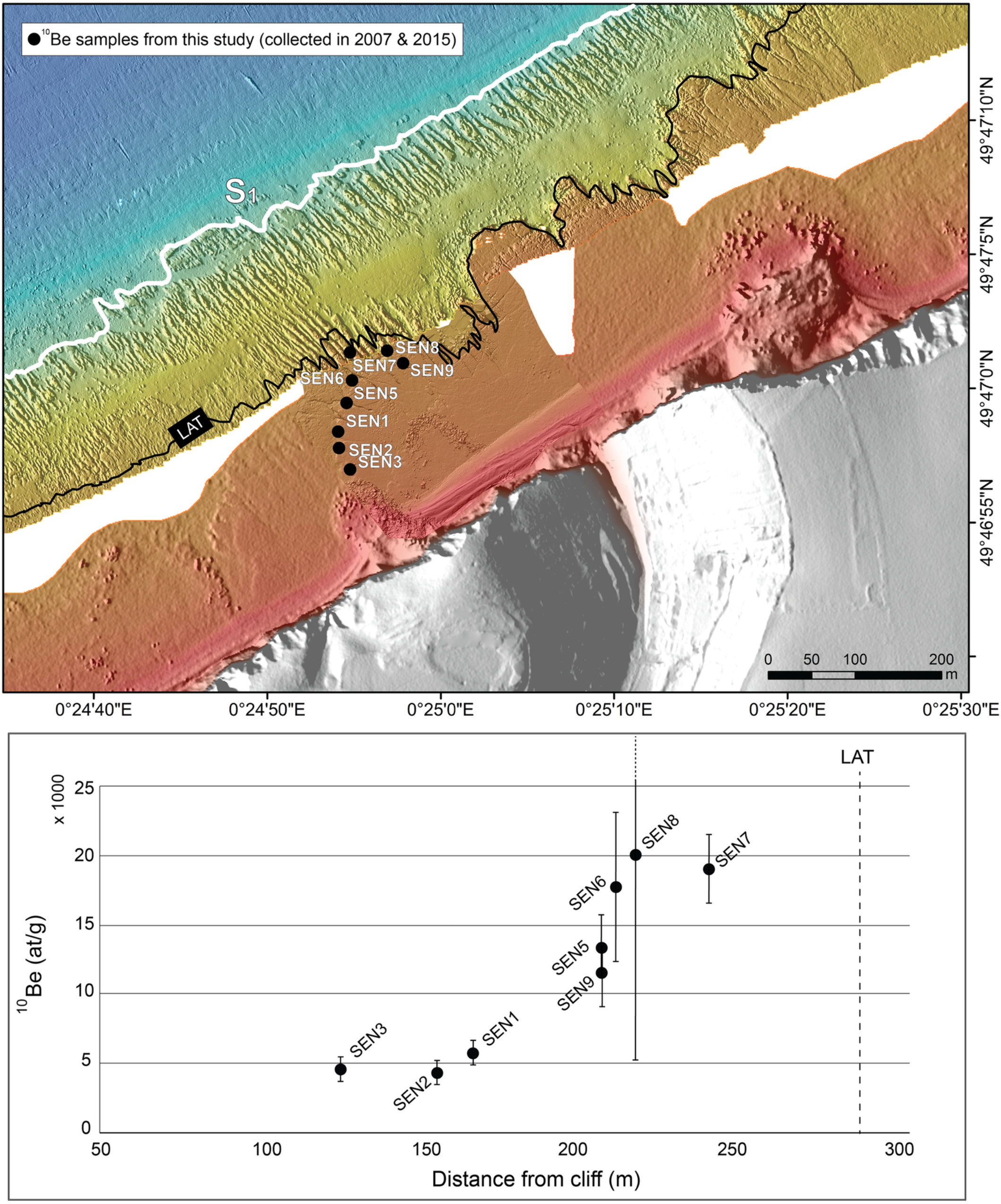

10Be samples from this study (collected in 2007 & 2015)
S1
LAT
SEN8
SEN7
SEN9
SEN6
SEN5
SEN1
SEN2
SEN3
49°47'10"N
49°47'5"N
49°47'0"N
49°46'55"N
0 50 100 200 m
0°24'40"E
0°24'50"E
0°25'0"E
0°25'10"E
0°25'20"E
0°25'30"E
LAT
x 1000
10Be (at/g)
Distance from cliff (m)

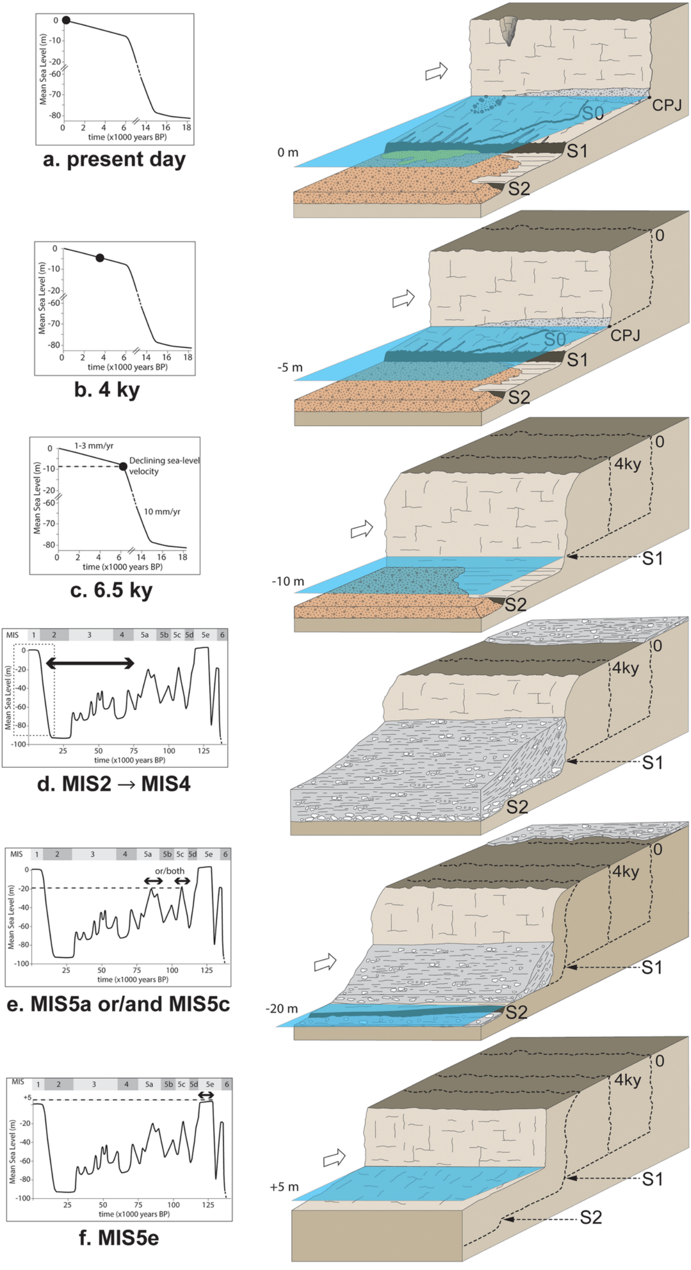
a. present day
b. 4 ky
c. 6.5 ky
d. MIS2 → MIS4
e. MIS5a or/and MIS5c
f. MIS5e
Mean Sea Level (m)
time (x1000 years BP)
1-3 mm/yr
Declining sea-level velocity
10 mm/yr
MIS
or/both
0 m
-5 m
-10 m
-20 m
+5 m
S0
S1
S2
CPJ
0
4ky

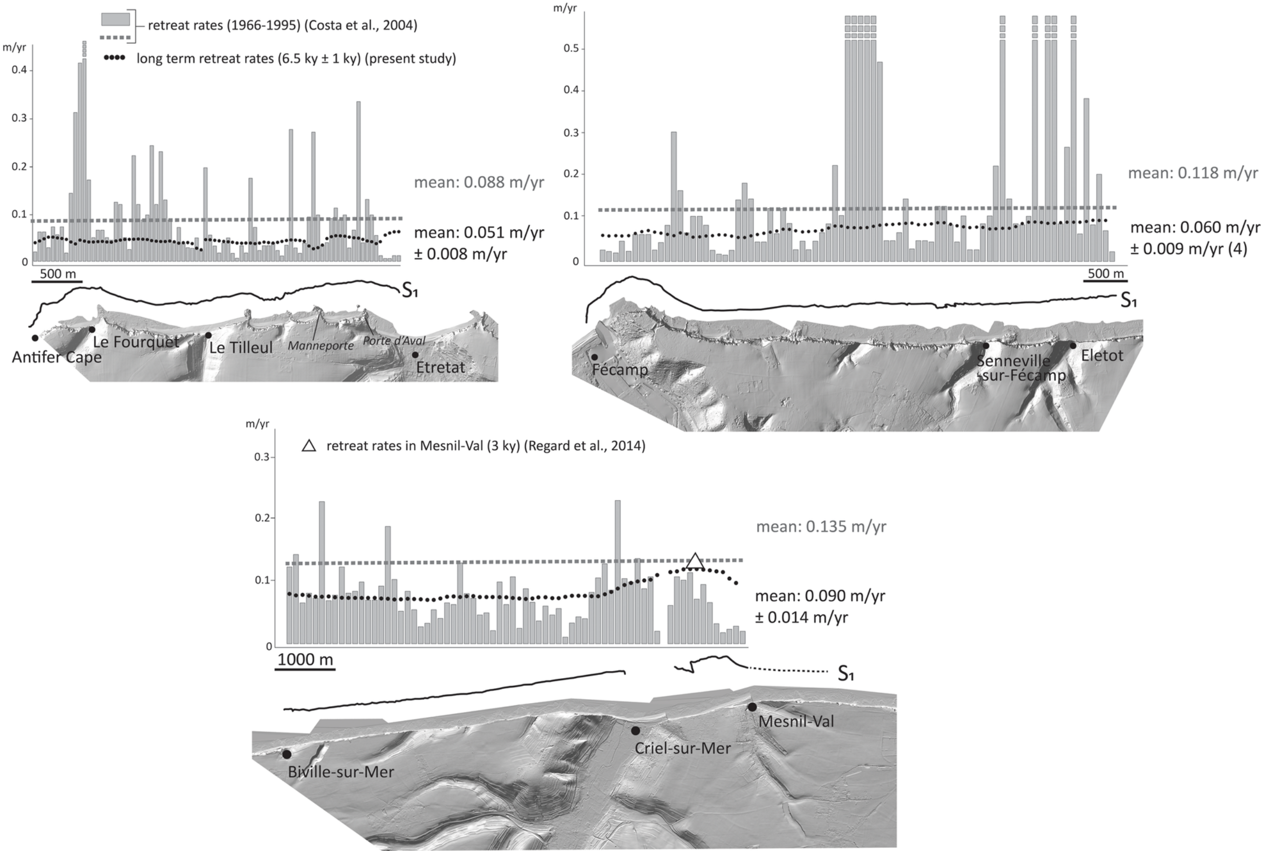

retreat rates (1966-1995) (Costa et al., 2004)
long term retreat rates (6.5 ky ± 1 ky) (present study)
m/yr
0.4
0.3
0.2
0.1
0
mean: 0.088 m/yr
mean: 0.051 m/yr
± 0.008 m/yr
500 m
S1
Antifer Cape
Le Fourquet
Le Tilleul
Manneporte
Porte d'Aval
Etretat
m/yr
0.5
0.4
0.3
0.2
0.1
0
mean: 0.118 m/yr
mean: 0.060 m/yr
± 0.009 m/yr (4)
500 m
S1
Fécamp
Senneville
sur-Fécamp
Eletot
m/yr
retreat rates in Mesnil-Val (3 ky) (Regard et al., 2014)
0.3
0.2
0.1
0
mean: 0.135 m/yr
mean: 0.090 m/yr
± 0.014 m/yr
1000 m
S1
Mesnil-Val
Criel-sur-Mer
Biville-sur-Mer

| Location | Stage | Local formation name | Uniform formation name | D.I (a.u) | ϕ (%) | K (mD) | UCS (MPa) | Microtextures | Ref. |
|---|---|---|---|---|---|---|---|---|---|
| Quiberville FR | Campanian | Newhaven Chalk Fm | Newhaven Chalk Fm | - | 36 | - | 3 | - | [1] |
| Newhaven UK | Campanian | Newhaven Chalk Fm | Newhaven Chalk Fm | 2 | 35.5 | 2.35 | - | MT1 | [2] |
| Coquelles Quarry FR | Santonian | Caffier Fm | Seaford Chalk Fm | 1 | 42.9 | 5.83 | 5 | MT1 | [2] |
| Seven Sister UK | Coniacien | White Chalk group | Seaford Chalk Fm | 1.5 | 40.2 | 3.1 | 4 | MT1 | [2] |
| Bois de Cise FR | Coniacian | Seaford Chalk Fm | Seaford Chalk Fm | - | 46 | - | 3 | - | [1] |
| Dieppe FR | Coniacien | Seaford Chalk Fm | Seaford Chalk Fm | - | 34 | - | 1 | - | [1] |
| Etretat FR | Coniacien | Craie de St-Pierre en Port | Lewes Nodular Chalk Fm | 2 | 33.8 | 13.3 | 3 | MT1 | [2] |
| Bois de Cise FR | Coniacian | Lewes Nodular Chalk Fm | Lewes Nodular Chalk Fm | - | 41 | 20 | 4 | - | [1] |
| Mimoyecques Quarry FR | Turonian | Guet Fm | Lewes Nodular Chalk Fm | 1 | 39.7 | 3.67 | 8 | MT1 | [2] |
| Mimoyecques Quarry FR | Turonian | Guet Fm | Lewes Nodular Chalk Fm | 1 | 43.6 | 4.32 | 4 | MT1 | [2] |
| Eletot FR | Turonian | Lewes Nodular Chalk Fm | Lewes Nodular Chalk Fm | - | 33 | - | 4 | MT1 | [1] |
| Birling Gap UK | Turonian | New Pit Chalk Fm | New Pit Chalk Fm | 1 | 37.8 | 3.09 | 5 | MT1 | [2] |
| Senneville-sur-Fecamp FR | Turonian | Craie de Senneville | New Pit Chalk Fm | 1 | 36.4 | 1.32 | 12 | MT1 | [2] |
| Senneville-sur-Fecamp FR | Turonian | Craie de Senneville | New Pit Chalk Fm | 1.5 | 40.4 | 2.68 | 10 | MT1 | [2] |
| Eastbourne UK | Turonian | Holywell Nodular Chalk Fm | Holywell Nodular Chalk Fm | 5 | 14.5 | 0.25 | 31 | MT2 | [2] |
| Saint Martin en Campagne FR | Turonian | Holywell Nodular Chalk Fm | Holywell Nodular Chalk Fm | 6 | 23.8 | 0.44 | 21 | MT2 | [2] |
| Saint Martin en Campagne FR | Turonian | Holywell Nodular Chalk Fm | Holywell Nodular Chalk Fm | 3.5 | 33 | 0.48 | - | MT2 | [2] |
| Saint Martin en Campagne FR | Turonian | Holywell Nodular Chalk Fm | Holywell Nodular Chalk Fm | 3 | 25.4 | 0.4 | 19 | MT2 | [2] |
| Cap Blanc Nez FR | Turonian | Grand Blanc Nez Fm | Holywell Nodular Chalk Fm | 4.5 | 20.7 | 0.19 | - | MT2 | [2] |
| Cap Blanc Nez FR | Turonian | Grand Blanc Nez Fm | Holywell Nodular Chalk Fm | 3 | 17.6 | 0.4 | 20 | MT2 | [2] |
| Eastbourne UK | Cenomanian | Zig-Zag Fm | Craie de Rouen | 6 | 14.2 | 0.06 | 35 | MT5 | [2] |
| Port of Antifer FR | Cenomanian | Craie de Rouen | Craie de Rouen | - | 35 | 0.16 | - | - | [1] |
| Cap Blanc Nez FR | Cenomanian | Escalles Fm | Craie de Rouen | 1.5 | 36.5 | - | 9 | MT1 | [2] |
| Cap Blanc Nez FR | Cenomanian | Escalles Fm | Craie de Rouen | 1 | 35.7 | 0.67 | 7 | MT1 | [2] |
| Cap Blanc Nez FR | Cenomanian | Escalles Fm | Craie de Rouen | 5 | 27.1 | 0.43 | 20 | MT2 | [2] |
| Cap Blanc Nez FR | Cenomanian | Escalles Fm | Craie de Rouen | 2.5 | 25.6 | 0.36 | 11 | MT2 | [2] |
| Cap Blanc Nez FR | Cenomanian | Cran Fm | Craie de Rouen | 3.5 | 26.2 | 0.33 | 15 | MT2 | [2] |
| Cap Blanc Nez FR | Cenomanian | Cran Fm | Craie de Rouen | 4 | 23.2 | 0.08 | 15 | MT4 | [2] |
| Cap Blanc Nez FR | Cenomanian | Petit Blanc Nez Fm | Glauconitic Chalk | 4 | 22.1 | 0.08 | 27 | MT4 | [2] |
| Cap Blanc Nez FR | Cenomanian | Petit Blanc Nez Fm | Glauconitic Chalk | 4 | 24.8 | 0.04 | 15 | MT4 | [2] |
| Cap Blanc Nez FR | Cenomanian | Strouanne Fm | Glauconitic Chalk | 2.5 | 26 | 0.79 | 13 | MT4 | [2] |
| Cap Blanc Nez FR | Cenomanian | Strouanne Fm | Glauconitic Chalk | 3.5 | 20 | 0.11 | 24 | MT4 | [2] |
| Cap Blanc Nez FR | Cenomanian | Strouanne Fm | Glauconitic Chalk | 2.5 | 21.1 | 0.05 | 18 | MT4 | [2] |

| Sample name | distance from cliff (m) | Latitude (°) | Longitude (°) | Elevation (m, NGF) | Mass of pure flint dissolved (g) | Measured $^{10}Be/^{9}Be$ | Uncertainty $^{10}Be/^{9}Be$ (%) | $^{10}Be$ concentration (at/g) | +/- (at/g) |
|---|---|---|---|---|---|---|---|---|---|
| MEV3 | 814 | 50,0472 | 1,3171 | -9,8 | 15,73 | 1,0660E-14 | 18,61 | 17908 | 3970 |
| MEV2 | 728 | 50,0470 | 1,3185 | -7,9 | 16,57 | 6,4840E-15 | 35,38 | 2545 | 3792 |
| MEV1 | 658 | 50,046887 | 1,319811 | -6,1 | 11,76 | 1,2405E-14 | 26,05 | 32316 | 8420 |
| MV-08 | 635 | 50,0474 | 1,3208 | -5,1 | 29,18 | 6,6921E-15 | 10,49 | 1504 | 642 |
| MEV6 | 561 | 50,048441 | 1,323864 | -4,0 | 22,46 | 3,4450E-14 | 6,15 | 46359 | 2854 |
| MV-01 | 471 | 50,0462 | 1,3278 | -4,2 | 29,92 | 1,1257E-14 | 6,50 | 4568 | 640 |
| MEV4a | 456 | 50,047669 | 1,324893 | -3,9 | 19,27 | 1,43035E-14 | 11,93 | 11822 | 2793 |
| MEV4b | 456 | 50,047669 | 1,324893 | -3,9 | 13,09 | 1,1911E-14 | 18,02 | 27490 | 4953 |
| MV-02 | 416 | 50,0465 | 1,3273 | -3,0 | 24,78 | 9,7594E-15 | 8,03 | 4270 | 803 |
| MV-03 | 353 | 50,0467 | 1,3267 | -2,1 | 30,93 | 9,0181E-15 | 9,10 | 2950 | 667 |
| MV-04 | 313 | 50,0469 | 1,3264 | -1,8 | 31,73 | 9,1295E-15 | 8,28 | 2948 | 617 |
| MV-05 | 279 | 50,0476 | 1,3260 | -1,6 | 30,79 | 8,7347E-15 | 7,79 | 2768 | 595 |
| MV-06 | 231 | 50,0471 | 1,3250 | -0,9 | 29,91 | 9,7071E-15 | 6,86 | 3503 | 604 |
| MV-07 | 167 | 50,0476 | 1,3213 | -0,7 | 30,82 | 9,4628E-15 | 11,95 | 3255 | 844 |

| Sample name | distance from cliff (m) | Latitude (°) | Longitude (°) | Elevation (m, NGF) | Mass of pure flint dissolved (g) | Measured $^{10}Be/^{9}Be$ | Uncertainty $^{10}Be/^{9}Be$ (%) | $^{10}Be$ concentration (at/g) | +/- (at/g) |
|---|---|---|---|---|---|---|---|---|---|
| SEN7 | 239 | 49,7835 | 0,4150 | -2,7 | 29,56 | 1,9822E-14 | 16,50 | 18821 | 3394 |
| SEN8 | 216 | 49,7834 | 0,4155 | -2,0 | 6,91 | 2,2541E-14 | 36,27 | 19790 | 15547 |
| SEN6 | 210 | 49,7833 | 0,4151 | -1,7 | 11,79 | 8,3632E-15 | 37,82 | 17554 | 8243 |
| SEN9 | 206 | 49,7834 | 0,4156 | -1,1 | 22,69 | 1,3314E-14 | 25,28 | 11288 | 4879 |
| SEN5 | 206 | 49,7830 | 0,4150 | -0,9 | 14,78 | 7,9670E-15 | 25,85 | 13182 | 4311 |
| SEN1 | 166 | 49,7826 | 0,4149 | -0,8 | 31,85 | 1,3156E-14 | 9,54 | 5497 | 524 |
| SEN2 | 155 | 49,7825 | 0,4149 | -0,4 | 32,49 | 1,1088E-14 | 11,37 | 4096 | 466 |
| SEN3 | 125 | 49,7823 | 0,4150 | 0,2 | 30,60 | 1,1125E-14 | 14,91 | 4365 | 651 |